

Supporting Information

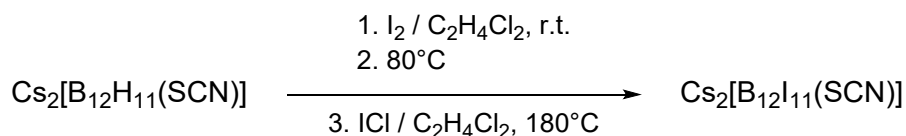
Generation and Reactivity of the Fragment Ion $[B_{12}I_8S(CN)]^-$ in the Gas Phase and on Surfaces

Sebastian Kawa, Jaskiran Kaur, Harald Knorke, Ziyang Warneke, Myriam Wadsack, Markus Rohdenburg, Marc Nierstenhöfer, Carsten Jenne, Hilikka Kenttämä, Jonas Warneke

Table of Contents

| | |
|--|----|
| 1 Synthetic details and characterization of $[Y]_2[B_{12}I_{11}(SCN)]$ ($Y = Cs^+, PPh_4$) | 1 |
| 2 Computational section | 7 |
| 3 Ion-molecule reactions with O_2 , N_2 and H_2O | 12 |
| 4 Ion-molecule reactions with cyclohexane, dimethyl sulfide and dimethyl amine | 14 |
| 4.2 Cyclohexane | 14 |
| 4.2 Dimethyl sulfide..... | 16 |
| 4.3 Dimethyl amine | 18 |
| 4.4 Without introduction of neutral reagent | 21 |
| 4.5 Comparison of cyclohexane, dimethyl sulfide, and dimethyl amine..... | 21 |
| 5 LESA mass spectrometry | 22 |
| 5.1 Background | 23 |
| 5.2 $[B_{12}I_{11}]^-$ | 23 |
| 5.3 $[B_{12}I_9]^-$ | 24 |
| 5.4 $[B_{12}I_8S(CN)]^-$ | 26 |
| 6 Ion soft-landing settings..... | 29 |
| 7 Measurement of kinetic energy..... | 30 |
| 8 References | 31 |

1 Synthetic details and characterization of $[Y]_2[B_{12}I_{11}(SCN)]$ ($Y = Cs^+$, PPh_4)



Dried $Cs_2[B_{12}H_{11}(SCN)]$ (0.31 g, 0.67 mmol, 1.0 eq.) and iodine (0.85 g, 3.35 mmol, 5.0 eq.) were dissolved in 1,2-dichloroethane (5 mL) in a 15 mL pressure tube. The tube was closed and the mixture was stirred for one hour at room temperature. Subsequently, the temperature was raised to 80 °C and the mixture was stirred for 90 min. After cooling to room temperature, the tube was carefully opened and iodine monochloride (0.52 mL, 9.90 mmol, 14.8 eq.) was added. The tube was closed again and heated to 180 °C for three days. The mixture was slowly cooled to room temperature. The residue was transferred onto a fine fit, washed with hexane (3 × 170 mL), and dried in vacuo, which gave 1.13 g of a pink crude product (as the Cs^+ salt). Purification could be achieved by a salt metathesis reaction in hot water with tetraphenylphosphonium chloride in 85% yielding of the corresponding $[PPh_4]^+$ salt. The product mixture contains the desired anion $[B_{12}I_{11}(SCN)]^{2-}$ as well as $[B_{12}I_{11}(SI)]^{2-}$ as a minor impurity, which could not be removed.

$^{11}B\{^1H\}$ NMR (192.59 MHz, CD_3CN): $\delta = -10.8$ (s, 1B, $[B_{12}I_{11}(SCN)]^{2-}$), -13.3 (s, $[B_{12}I_{11}(SI)]^{2-}$), -15.0 (s, 5B, $[B_{12}I_{11}(SCN)]^{2-}$), 16.6 (s, $[B_{12}I_{11}(SI)]^{2-}$), -17.3 (s, 6B, $[B_{12}I_{11}(SCN)]^{2-}$).

ESI-MS [m/z]: found = 380.7095 (calculated = 380.7134; I_3^-), 792.0023 (calculated = 792.0224; $[B_{12}I_{11}(SCN)]^{2-}$), 842.4527 (calculated = 842.4731; $[B_{12}I_{11}(SI)]^{2-}$), 1606.9896 (calculated = 1607.0333; $Na[B_{12}I_{11}(SCN)]^-$), 1716.9010 (calculated = 1716.9490; $Cs[B_{12}I_{11}(SCN)]^-$).

IR (diamond ATR) of $Cs_2[B_{12}I_{11}(SCN)]$: $\nu = 2142$ (m, $\nu(SC\equiv N)$), 1652 (vw), 1603 (w), 1404 (m), 1205 (w), 1153 (w), 981 (sh, w), 929 (vs, $\nu(B-I)$), 855 (sh, w), 799 (sh, w), 462 (w). Raman of $[PPh_4]_2[B_{12}I_{11}(SCN)]$: $\nu = 3059$ (m), 2147 (w, $\nu(SC\equiv N)$), 1586 (m), 1191 (w), 1167 (w), 1097 (w), 1028 (m), 1001 (s), 725 (w), 680 (w), 616 (w), 338 (w) 283 (w), 257 (m), 243 (m), 205 (w), 144 (vs), 94 (vs), 72 (vs).

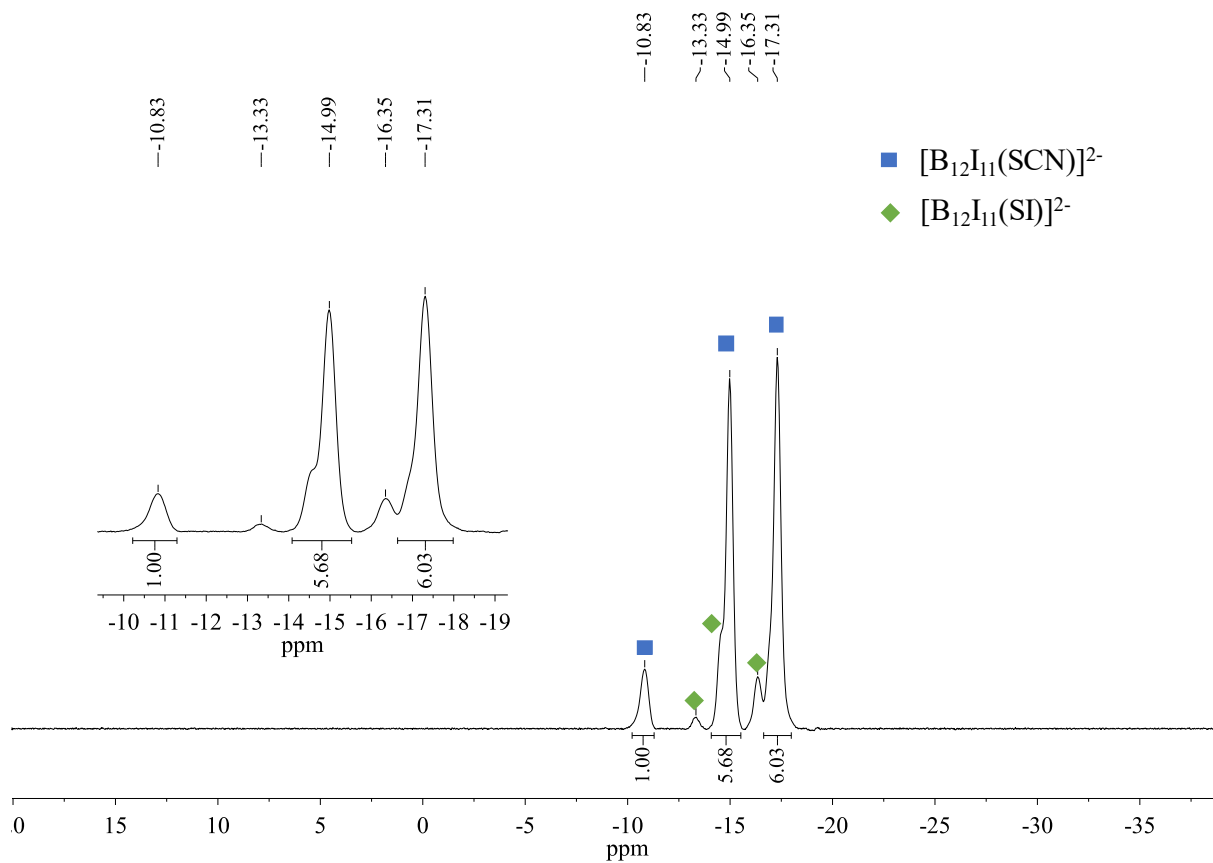


Figure S1. ^{11}B $\{^1\text{H}\}$ NMR spectrum (192.59 MHz, 298 K) of $\text{Cs}_2[\text{B}_{12}\text{I}_{11}(\text{SCN})]$ in CD_3CN .

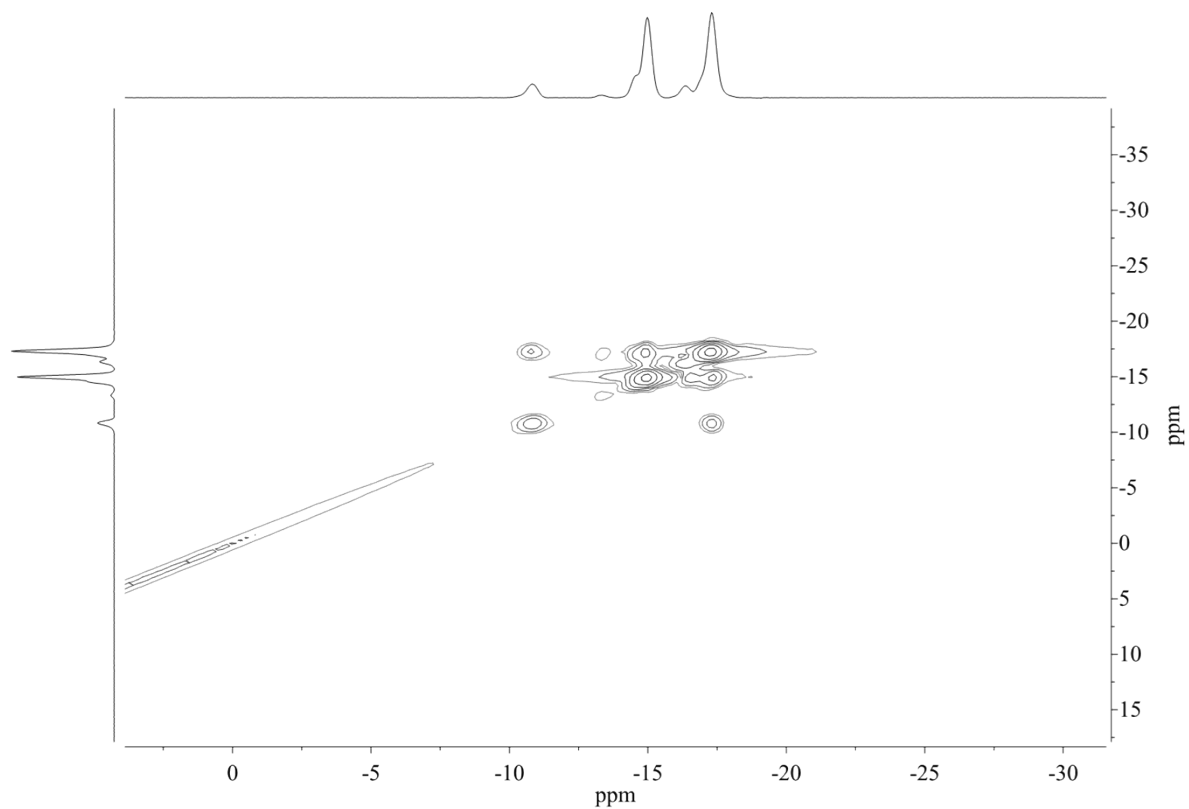


Figure S2. ^{11}B $\{^1\text{H}\}$ - ^{11}B $\{^1\text{H}\}$ COSY NMR spectrum (192.59 MHz, 298 K) of $\text{Cs}_2[\text{B}_{12}\text{I}_{11}(\text{SCN})]$ in CD_3CN .

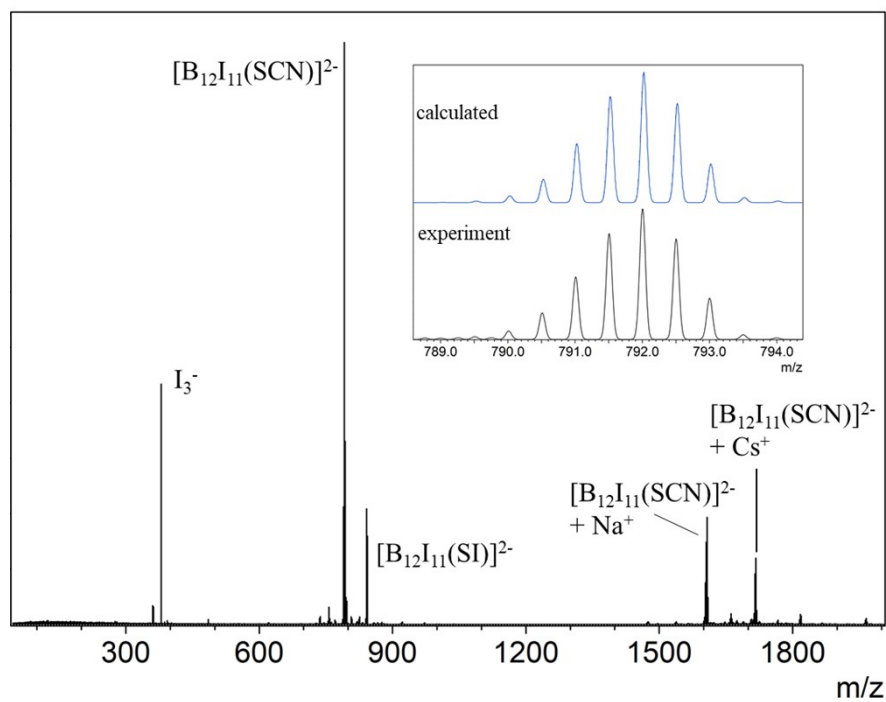


Figure S3. ESI mass spectrum (negative mode) of $\text{Cs}_2[\text{B}_{12}\text{I}_{11}(\text{SCN})]$. The simulated mass spectrum is shown above.

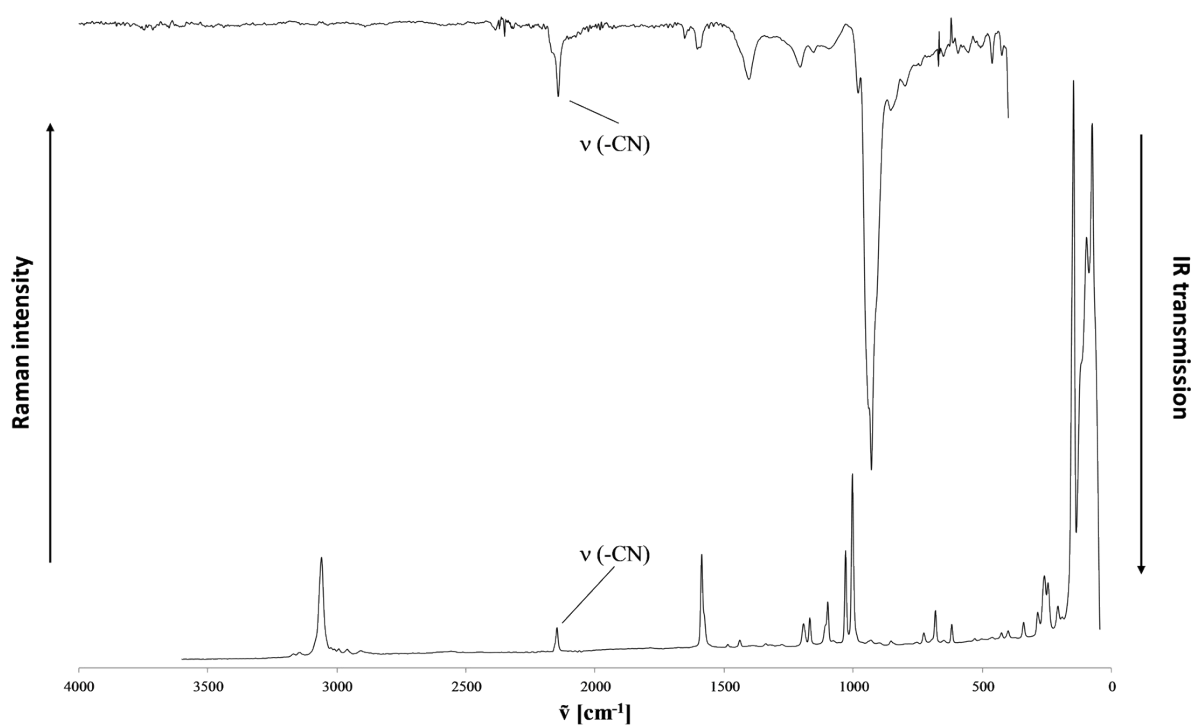


Figure S4. IR- (top) and Raman-spectra (bottom) of $\text{Cs}_2[\text{B}_{12}\text{I}_{11}(\text{SCN})]$ (top) and $[\text{PPh}_4]_2[\text{B}_{12}\text{I}_{11}(\text{SCN})]$ (bottom).

Table S1. Crystal data and structure refinement for [Cs₂(NCCH₃)₂][B₁₂I₁₁(SCN)].

| | |
|--|--|
| CCDC number | 2308756 |
| Empirical formula | C ₅ H ₆ B ₁₂ Cs ₂ I ₁₁ N ₃ S |
| Formula weight | 1931.63 |
| Temperature/K | 150 (1) |
| Crystal system | monoclinic |
| Space group | <i>I</i> 2/m |
| <i>a</i> /Å | 10.6637(2) |
| <i>b</i> /Å | 12.5200(3) |
| <i>c</i> /Å | 13.6723(3) |
| <i>α</i> /° | 90 |
| <i>β</i> /° | 99.352(2) |
| <i>γ</i> /° | 90 |
| Volume/Å ³ | 1801.12(7) |
| <i>Z</i> | 2 |
| ρ_{calc} /cm ³ | 3.562 |
| μ /mm ⁻¹ | 11.517 |
| F(000) | 1652.0 |
| Crystal size/mm ³ | 0.12 × 0.08 × 0.06 |
| Radiation | MoK α (λ = 0.71073) |
| 2 θ range for data collection/° | 6.508 to 52.998 |
| Index ranges | -13 ≤ <i>h</i> ≤ 10, -11 ≤ <i>k</i> ≤ 15, -17 ≤ <i>l</i> ≤ 17 |
| Reflections collected | 4454 |
| Independent reflections | 1934 [<i>R</i> _{int} = 0.0192, <i>R</i> _{sigma} = 0.0267] |
| Data/restraints/parameters | 1934/14/107 |
| Goodness-of-fit on <i>F</i> ² | 1.058 |
| Final <i>R</i> indexes [<i>I</i> ≥ 2 σ (<i>I</i>)] | <i>R</i> ₁ = 0.0299, <i>wR</i> ₂ = 0.0742 |
| Final <i>R</i> indexes [all data] | <i>R</i> ₁ = 0.0342, <i>wR</i> ₂ = 0.0762 |
| Largest diff. peak/hole / e Å ⁻³ | 1.50/-1.60 |

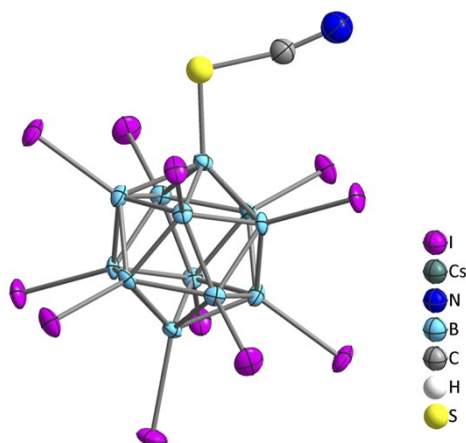


Figure S5. Part of the crystal structure of $\text{Cs}_2[\text{B}_{12}\text{I}_{11}(\text{SCN})] \cdot 2 \text{CH}_3\text{CN}$. Thermal ellipsoids are drawn with 50 % probability. Cations, solvent molecules and disorder are omitted for clarity. The sulfur atom could not be refined anisotropically.

Table S2. Fractional Atomic Coordinates ($\times 10^4$) and Equivalent Isotropic Displacement Parameters ($\text{\AA}^2 \times 10^3$). U_{eq} is defined as $1/3$ of the trace of the orthogonalized U_{ij} tensor.

| Atom | x | y | z | U_{eq} |
|------|-----------|-----------|------------|-----------------|
| Cs1 | 5000 | 2937.9(6) | 5000 | 57.3(3) |
| I2 | 3767.4(6) | 5000 | 7174.9(4) | 23.50(16) |
| I3 | 3463.0(4) | 2375.7(3) | 8904.5(3) | 24.33(13) |
| I4 | 8639.7(5) | 5000 | 10808.0(5) | 29.39(17) |
| N2 | 3235(9) | 5000 | 4527(7) | 38(2) |
| C2 | 2213(11) | 5000 | 4086(8) | 32(2) |
| C3 | 930(11) | 5000 | 3506(11) | 49(3) |
| B1 | 5849(6) | 4293(6) | 9287(4) | 14.0(12) |
| B2 | 4467(9) | 5000 | 8758(6) | 12.9(17) |
| B3 | 4335(6) | 3841(5) | 9515(4) | 13.2(12) |
| B4 | 6603(8) | 5000 | 10364(7) | 15.4(18) |
| I1 | 6929.2(8) | 3380.1(7) | 8344.6(6) | 25.30(19) |
| S1 | 7067(9) | 3589(8) | 8580(7) | 15(2) |
| N1 | 5690(30) | 2450(30) | 7060(20) | 68(10) |
| C1 | 6100(40) | 3010(40) | 7700(30) | 73(12) |

Table S3. Bond lengths.

| Atom | Atom | Length/Å | Atom | Atom | Length/Å |
|------|-----------------|-----------|------|-----------------|-----------|
| Cs1 | I4 ¹ | 4.1684(8) | C2 | C3 | 1.466(16) |
| Cs1 | I4 ² | 4.1684(8) | B1 | B1 ⁶ | 1.770(14) |
| Cs1 | N2 | 3.199(5) | B1 | B2 | 1.770(10) |
| Cs1 | N2 ³ | 3.199(6) | B1 | B3 | 1.785(9) |
| Cs1 | I1 ² | 4.0200(9) | B1 | B3 ⁷ | 1.773(9) |
| Cs1 | I1 ⁴ | 4.0200(9) | B1 | B4 | 1.793(10) |
| Cs1 | S1 ⁴ | 3.903(10) | B1 | I1 | 2.186(6) |
| Cs1 | S1 ² | 3.903(10) | B1 | S1 | 1.951(11) |
| Cs1 | N1 ⁵ | 2.86(3) | B2 | B3 | 1.801(8) |
| Cs1 | N1 | 2.86(3) | B2 | B3 ⁶ | 1.801(8) |
| Cs1 | C1 ⁵ | 3.69(3) | B2 | B4 ⁸ | 1.785(13) |
| Cs1 | C1 | 3.69(3) | B3 | B3 ⁷ | 1.776(12) |
| I2 | B2 | 2.172(8) | B3 | B4 ⁸ | 1.786(8) |
| I3 | B3 | 2.162(6) | S1 | C1 | 1.622(18) |
| I4 | B4 | 2.158(9) | N1 | C1 | 1.153(19) |
| N2 | C2 | 1.156(14) | | | |

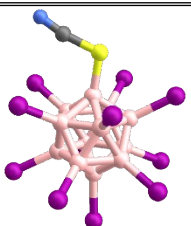
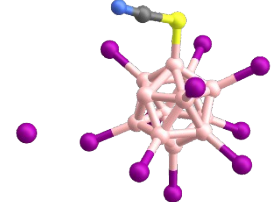
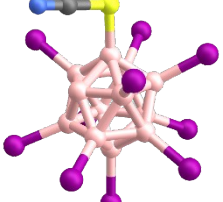
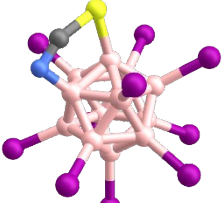
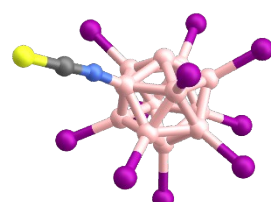
| | |
|---|-------------------------|
| 1 | -1/2+X, -1/2+Y, -1/2+Z; |
| 2 | 3/2-X, 1/2-Y, 3/2-Z |
| 3 | 1-X, 1-Y, 1-Z |
| 4 | -1/2+X, 1/2-Y, -1/2+Z |
| 5 | 1-X, +Y, 1-Z |
| 6 | +X, 1-Y, +Z |
| 7 | 1-X, +Y, 2-Z |
| 8 | 1-X, 1-Y, 2-Z |

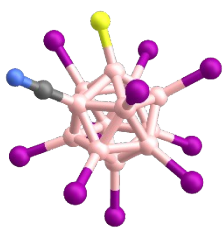
2 Computational section

Table S4. Calculated 0 K attachment enthalpies in kJ mol^{-1} (B3LYP-GD3BJ/def2TZVPP) for the reaction with N_2 .

| Ion | $\Delta H^{0\text{K}}$ |
|---|------------------------|
| $[\text{B}_{12}\text{I}_{10}\text{SCN}]^- + \text{N}_2$ | 140.5 |
| $[\text{B}_{12}\text{I}_{11}]^- + \text{N}_2$ | 137.3 |

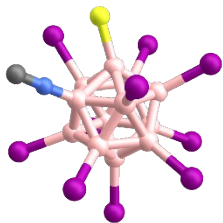
Table S5. Computed (B3LYP-GD3BJ/def2TZVPP) Coulomb barrier for the iodide loss of $[\text{B}_{12}\text{I}_{11}(\text{SCN})]^{2-}$ and iodide attachment enthalpies (BSSE and ZPE corrected) of different $[\text{B}_{12}\text{I}_{10}\text{SCN}]^-$ isomers.

| Picture | Description | Relative energy / kJ mol^{-1} |
|---|--|--|
|  | $\text{B}_{12}\text{I}_{11}(\text{SCN})$ | 0 |
|  | Coulomb barrier | +314 |
|  | SCN | +175 |
|  | bridged | +105 |
|  | NCS | +103 |



divided to S and CN

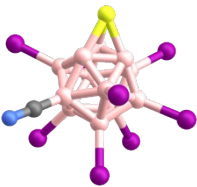
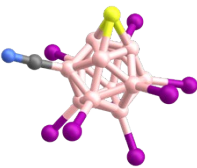
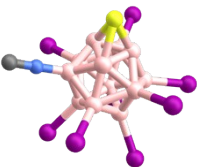
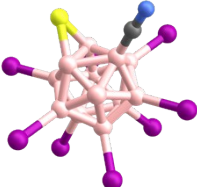
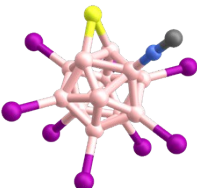
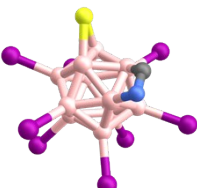
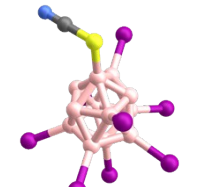
+93



divided to S and NC

+124

Table S6. Different computed isomers of $[\text{B}_{12}\text{I}_8\text{SCN}]^-$ (B3LYP-GD3BJ/def2TZVPP) and relative 0 K enthalpies.

| Picture | Description | Relative enthalpie / kJ mol^{-1} |
|---|--|---|
|  | $\text{B}_{12}\text{I}_8\text{S}(\text{CN})$ | 0 |
|  | Different (CN)-position | +2* |
|  | (NC)-group | +35 |
|  | Vacant boron | +119 |
|  | Vacant boron, (NC)-group | +150 |
|  | Bridging (CN) | +231 |
|  | Three vacant borons | +276 |

*Although this isomer is 2 kJ mol^{-1} higher in energy than the upper displayed isomer, it is shown in Figure 1, Scheme 1, and Table S7, because the calculated dissociation pathway discussed in the manuscript resulted in this isomer. The energy difference of 2 kJ mol^{-1} is within the uncertainty of the DFT calculations.

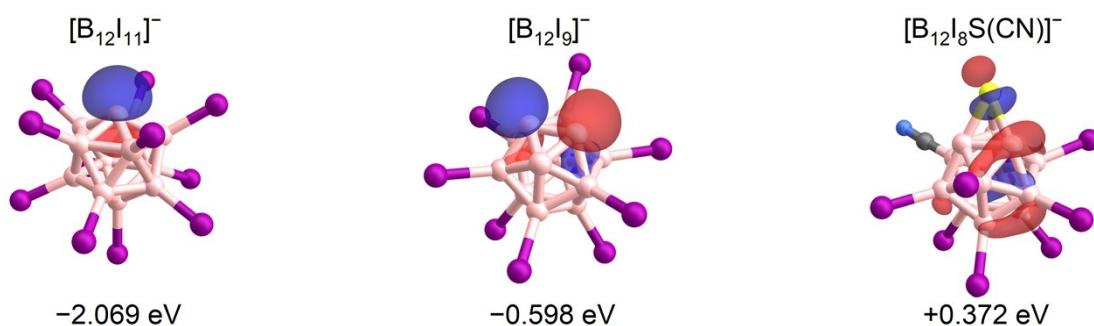


Figure S6. Visualized lowest unoccupied molecular orbitals (iso value: 0.05 a.u.) and computed energy levels (B3LYP-GD3BJ/def2TZVPP) of $[B_{12}I_{11}]^-$, $[B_{12}I_9]^-$, and $[B_{12}I_8S(CN)]^-$.

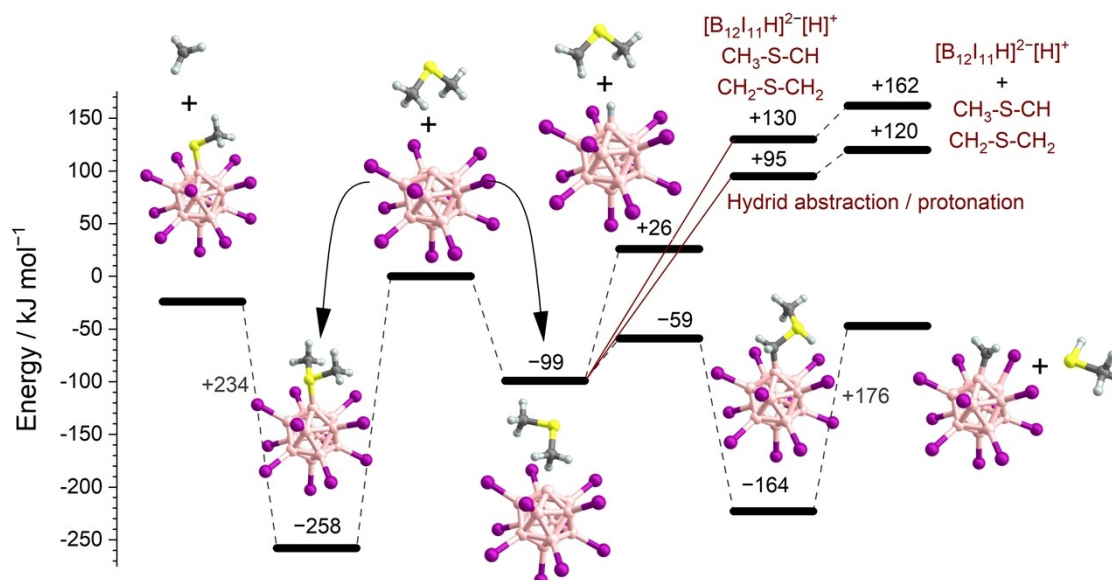


Figure S7. Reaction pathway (B3LYP-GD3BJ/def2TZVPP) for the addition of $S(CH_3)_2$ to $[B_{12}I_{11}]^-$ and the proposed generation of $[B_{12}I_{11}H]^{2-}$. The reaction pathway from the stable reaction product at -99 kJ mol^{-1} to the hydride abstraction / protonation product at $+130 (+95) \text{ kJ mol}^{-1}$ requires overcoming a barrier (transition state), which is not shown here.

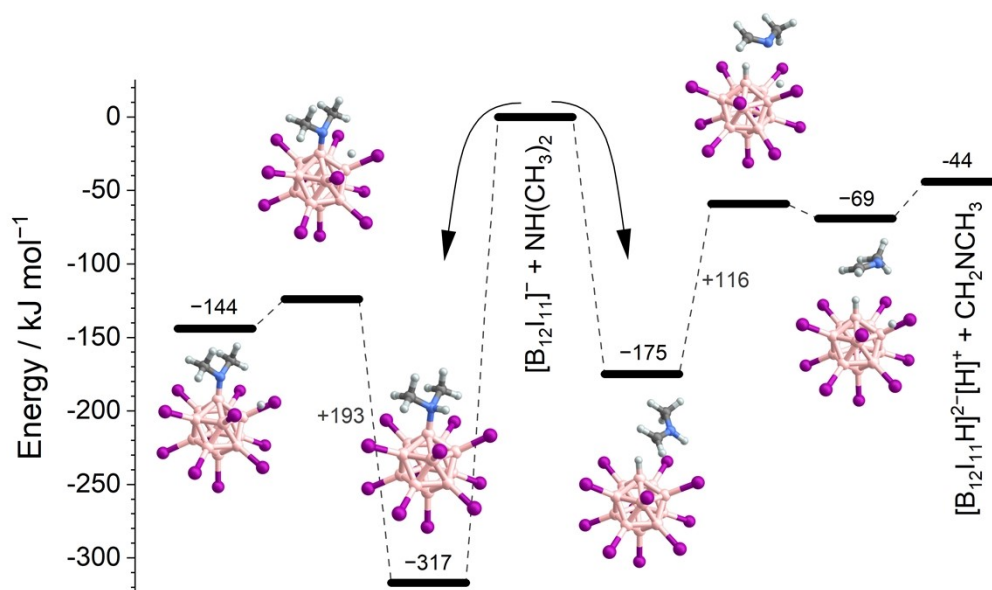
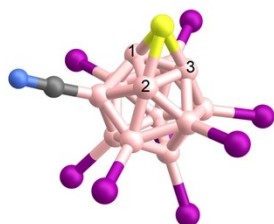


Figure S8. Reaction pathway (B3LYP-GD3BJ/def2TZVPP) for the addition of $\text{HN}(\text{CH}_3)_2$ to $[\text{B}_{12}\text{I}_{11}]^-$ and the proposed hydride abstraction / protonation sequence.

Table S7. Atomic charge derived from natural population analysis (NPA) (B3LYP-GD3BJ/def2TZVPP).

| Vacant / sulfur-bridged boron atoms in $[\text{B}_{12}\text{I}_n]^-$ / $[\text{B}_{12}\text{I}_8\text{S}(\text{CN})]^-$ | NPA charge / e |
|---|----------------|
| B_1 ($n = 11$) | 0.802 |
| B_1 ($n = 9$) | 0.039 |
| B_2 ($n = 9$) | 0.039 |
| B_3 ($n = 9$) | 0.039 |
| B_1 | -0.107 |
| B_2 | -0.107 |
| B_3 | -0.144 |
| S | 0.336 |



Note that coordinates can be found under the following link:
<https://iochem-bd.bsc.es/browse/handle/100/314968>

3 Energy resolved relative abundances of fragment ions and precursor ions

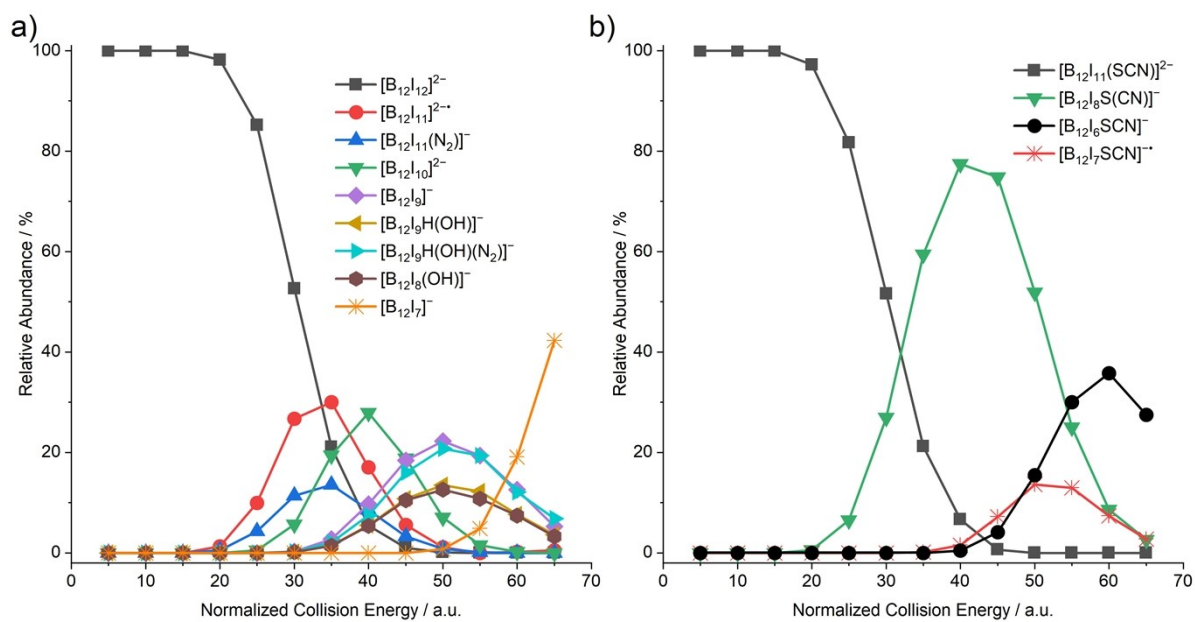


Figure S9. Diagrams showing the relative abundances of fragment ions and precursor ions generated by isolation and subsequent fragmentation of **a)** $[B_{12}I_{12}]^{2-}$ ions and **b)** $[B_{12}I_{11}SCN]^{2-}$ ions as a function of the normalized collision energy. Note that for reasons of clarity, only ions with a relative abundance larger than 12% of the total ion abundance are displayed.

4 Ion-molecule reactions with O₂, N₂ and H₂O

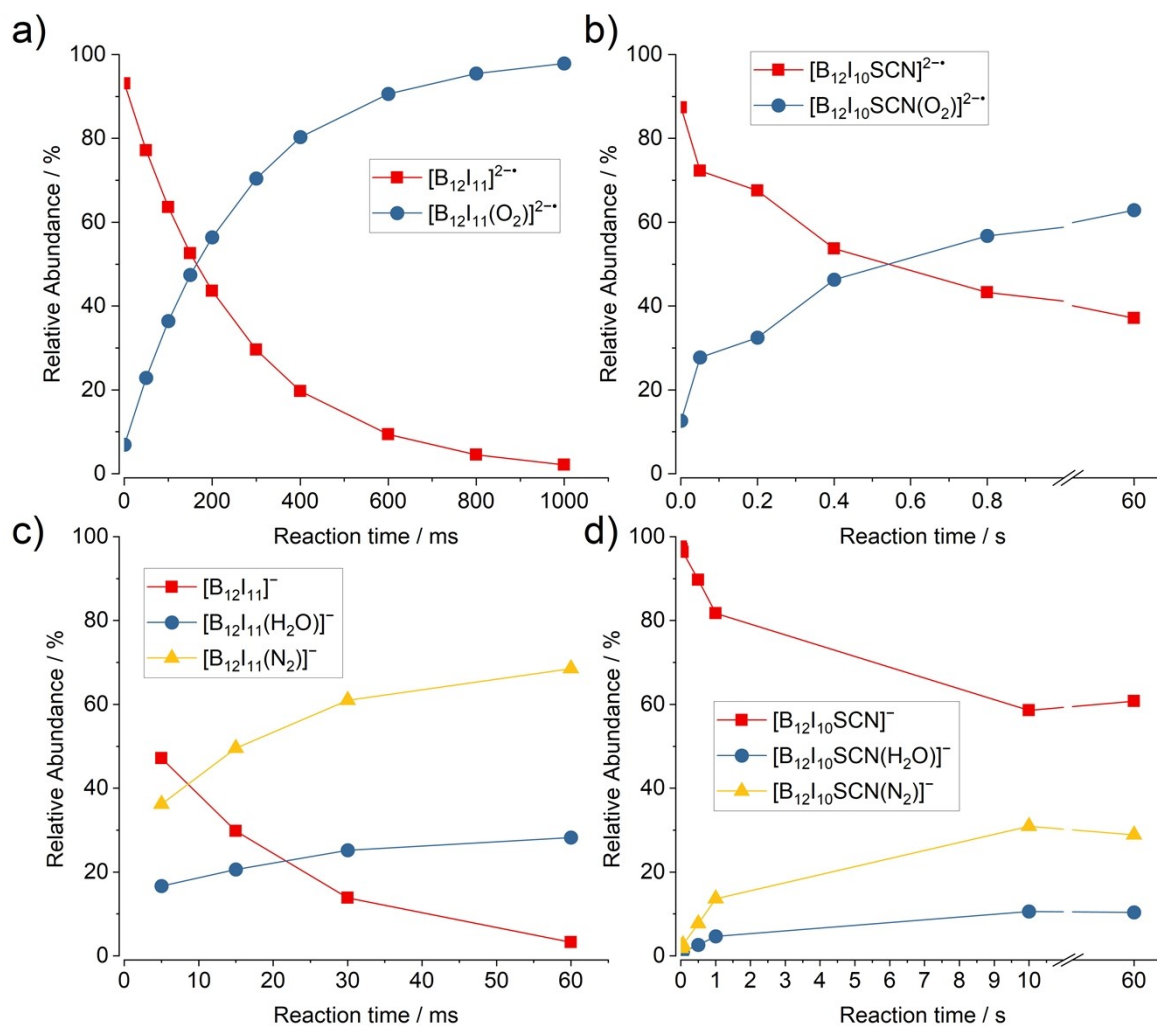


Figure S10. Plot of the relative abundance of the isolated ion and its ionic reaction products with background gas molecules as a function of the reaction time (instrumental parameter: activation time, time before ions are ejected out of the ion trap). **a)** $[B_{12}l_{11}]^{2-}$ in red color and $[B_{12}l_{11}(O_2)]^{2-}$ in blue color. **b)** $[B_{12}l_{10}SCN]^{2-}$ in red color and $[B_{12}l_{10}SCN(O_2)]^{2-}$ in blue color. **c)** $[B_{12}l_{11}]^{-}$ in red color, $[B_{12}l_{11}(H_2O)]^{-}$ in blue color, and $[B_{12}l_{11}(N_2)]^{-}$ in yellow color. **d)** $[B_{12}l_{10}SCN]^{-}$ in red color, $[B_{12}l_{10}SCN(H_2O)]^{-}$ in blue color, and $[B_{12}l_{10}SCN(N_2)]^{-}$ in yellow color.

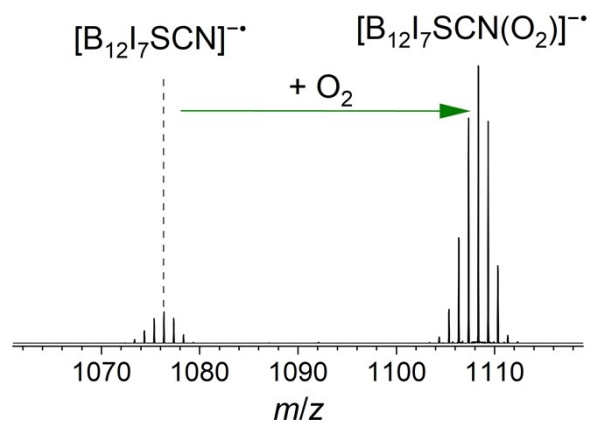


Figure S11. Section of a CID MS² mass spectrum measured (LTQ XL orbitrap) after isolation and fragmentation of $[B_{12}I_{11}SCN]^{2-}$ ions (m/z 1203, CID 50) and subsequent isolation of $[B_{12}I_7SCN]^-$ ions (m/z 1076) for a reaction time of 30 ms. The green arrow highlights the O_2 addition.

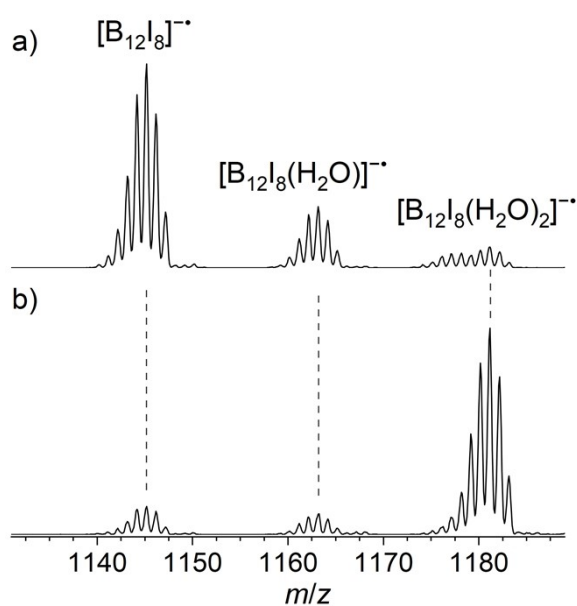


Figure S12. Section of a CID MS² mass spectrum measured (LTQ XL orbitrap, analyzer: ion trap) after in-source fragmentation of ESI-generated ions from the $K_2[B_{12}I_{12}]$ solution (CID 50) and subsequent isolation of $[B_{12}I_8]^-$ ions (m/z 1145) for a reaction time of **a)** 30 ms and **b)** 200 ms.

5 Ion-molecule reactions with cyclohexane, dimethyl sulfide and dimethyl amine
5.2 Cyclohexane

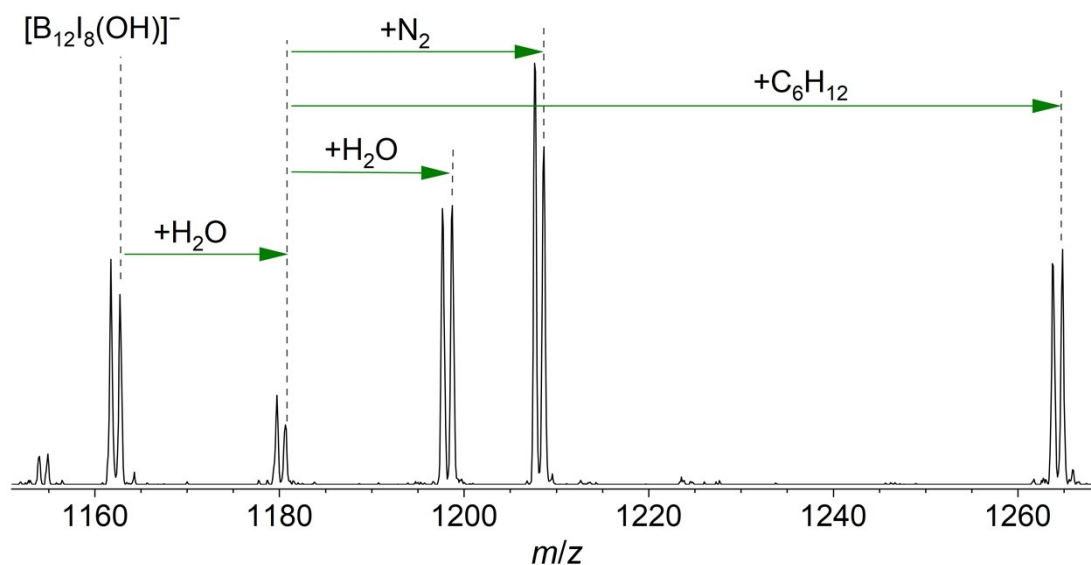


Figure S13. Section of a CID MS³ mass spectrum measured after in-source fragmentation of ESI-generated ions from the $K_2[B_{12}I_{12}]$ solution (CID 35), subsequent isolation of $[B_{12}I_9]^-$ ions (m/z 1272) for a reaction time of 300 ms, and the following isolation of $[B_{12}I_8(OH)]^-$ ions (m/z 1162) for a reaction time of 30 ms with cyclohexane and residual gas. Green arrows highlight addition reactions.

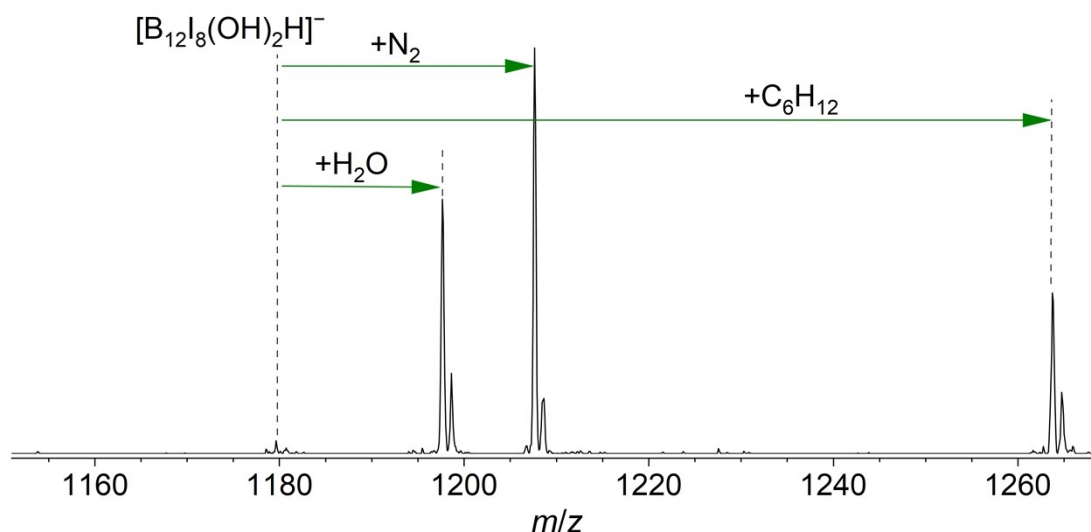


Figure S14. Section of a CID MS³ mass spectrum measured after in-source fragmentation of ESI-generated ions from the $K_2[B_{12}I_{12}]$ solution (CID 40), subsequent isolation of $[B_{12}I_8(OH)]^-$ ions (m/z 1162) for a reaction time of 300 ms, and the following isolation of $[B_{12}I_8(OH)_2H]^-$ ions (m/z 1180) for a reaction time of 100 ms with cyclohexane and residual gas. Green arrows highlight addition reactions.

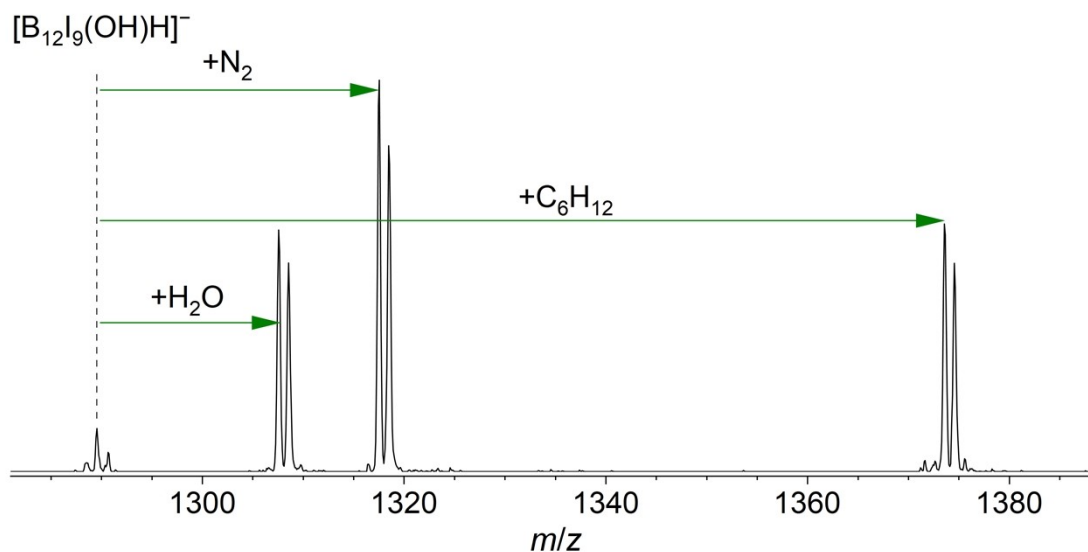


Figure S15. Section of a CID MS³ mass spectrum measured after in-source fragmentation of ESI-generated ions from the $K_2[B_{12}I_{12}]$ solution (CID 35), subsequent isolation of $[B_{12}I_9]^-$ ions (m/z 1272) for a reaction time of 300 ms, and the following isolation of $[B_{12}I_9(OH)H]^-$ ions (m/z 1290) for a reaction time of 30 ms with cyclohexane and residual gas. Green arrows highlight addition reactions.

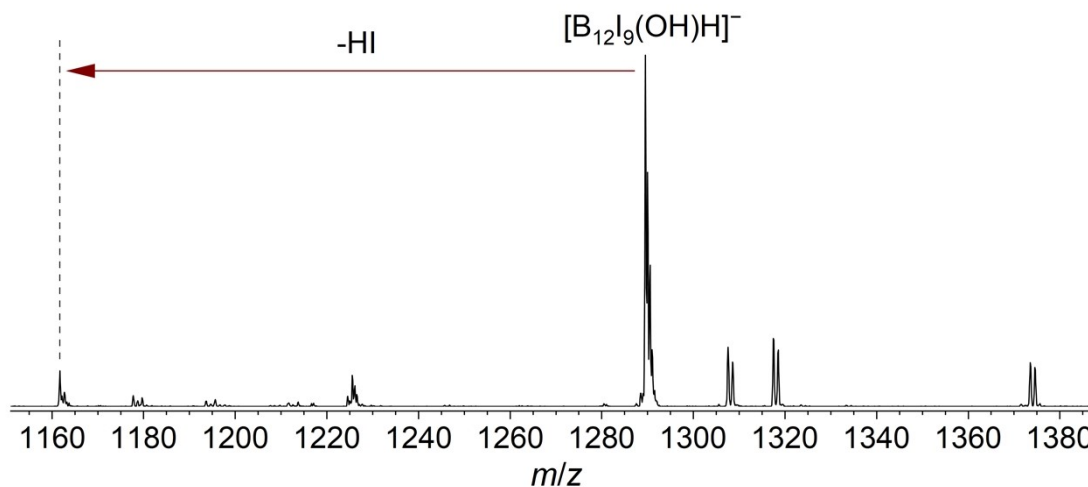


Figure S16. Section of a CID MS² mass spectrum measured after in-source fragmentation of ESI-generated ions from the $K_2[B_{12}I_{12}]$ solution (CID 40) and subsequent isolation and fragmentation of $[B_{12}I_9(OH)H]^-$ ions (m/z 1290) upon CID at a collision energy of 15 arbitrary units. The reagent was cyclohexane. The red arrow highlights the elimination of HI.

5.2 Dimethyl sulfide

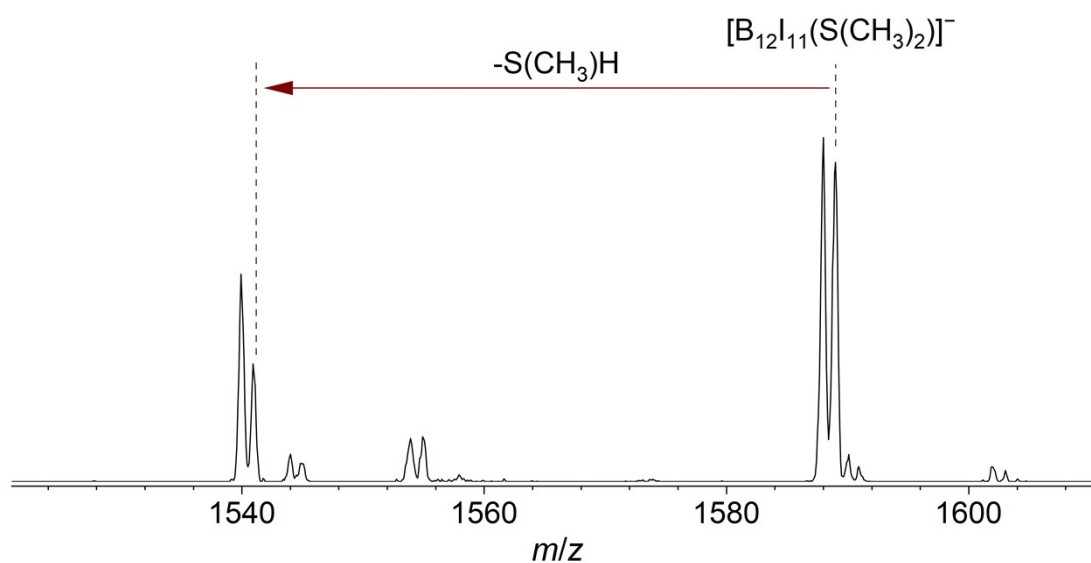


Figure S17. Section of a CID MS^3 mass spectrum measured after in-source fragmentation of ESI-generated ions from the $K_2[B_{12}I_{12}]$ solution (CID 40), subsequent isolation of $[B_{12}I_{11}]^-$ ions (m/z 1526) for a reaction time of 100 ms and the following isolation and fragmentation of $[B_{12}I_{11}(S(CH_3)_2)]^-$ ions (m/z 1588) upon CID at a collision energy of 20 arbitrary units. The reagent was dimethyl sulfide. The red arrow highlights the elimination of $S(CH_3)H$.

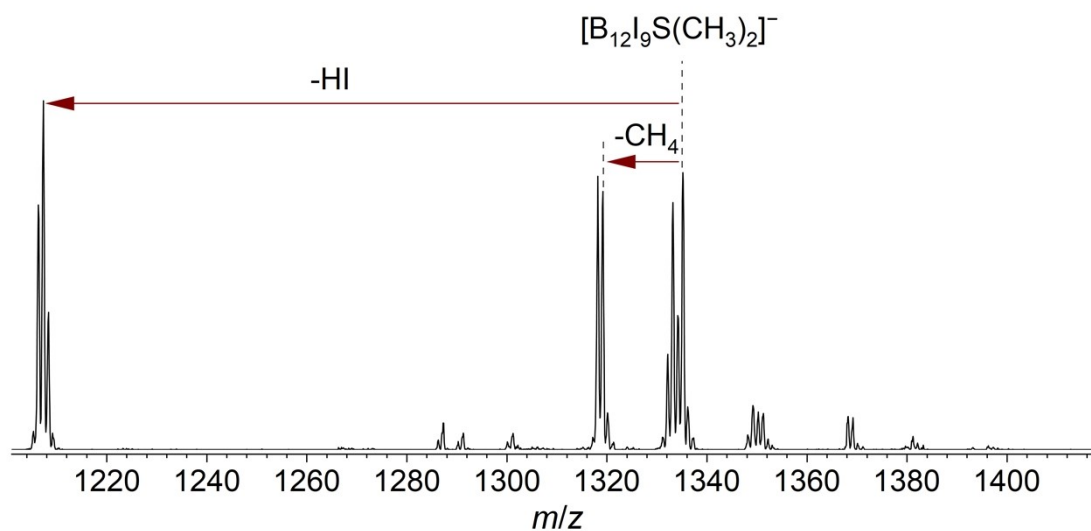


Figure S18. Section of a CID MS^3 mass spectrum measured after in-source fragmentation of ESI-generated ions from the $K_2[B_{12}I_{12}]$ solution (CID 40), subsequent isolation of $[B_{12}I_9]^-$ ions (m/z 1272) for a reaction time of 30 ms, and the following isolation and fragmentation of $[B_{12}I_9(S(CH_3)_2)]^-$ ions (m/z 1335) upon CID at a collision energy of 20 arbitrary units. The reagent was dimethyl sulfide. The red arrows highlight the eliminations of CH_4 and HI .

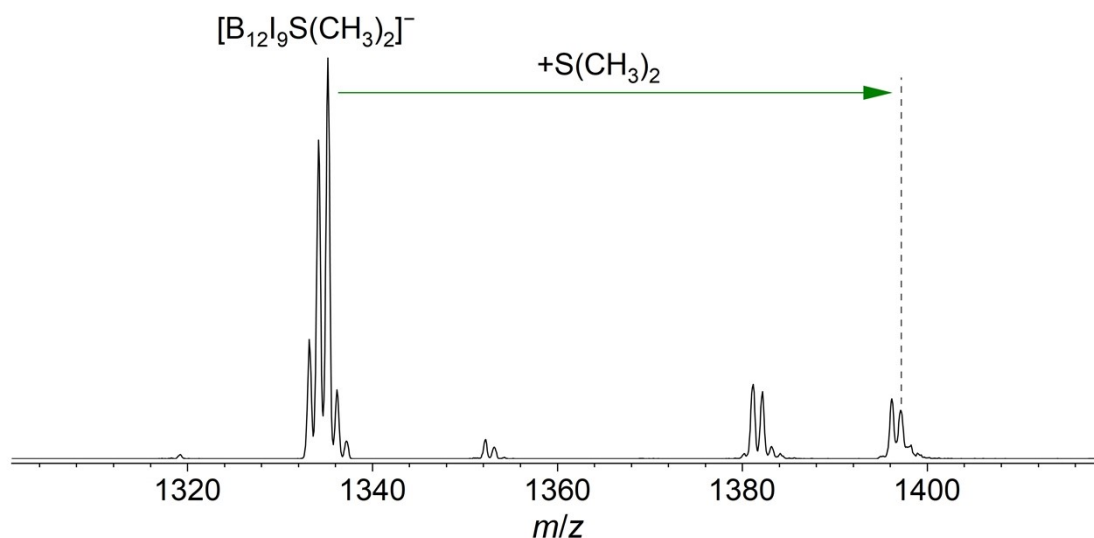


Figure S19. Section of a CID MS³ mass spectrum measured after in-source fragmentation of ESI-generated ions from the K₂[B₁₂I₁₂] solution (CID 40), subsequent isolation of [B₁₂I₉]⁻ ions (m/z 1272) for a reaction time of 30 ms, and the following isolation of [B₁₂I₉S(CH₃)₂]⁻ ions (m/z 1335) for a reaction time of 30 ms with dimethyl sulfide and residual gas. The green arrow highlights the addition reaction with a second dimethyl sulfide molecule.

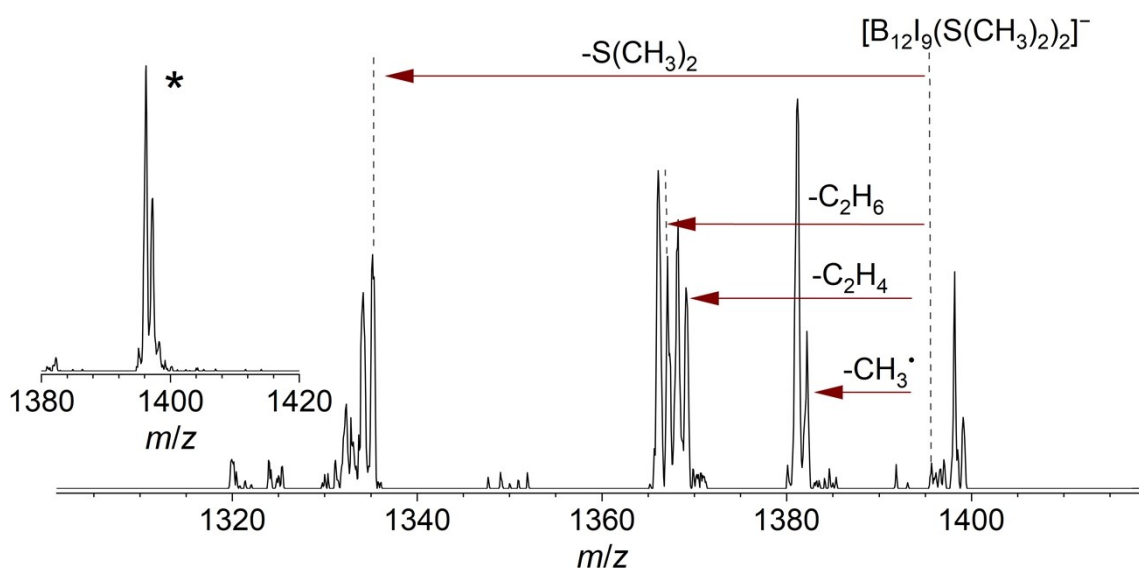


Figure S20. Section of a CID MS³ mass spectrum measured after in-source fragmentation of ESI-generated ions from the K₂[B₁₂I₁₂] solution (CID 40), subsequent isolation of [B₁₂I₉]⁻ ions (m/z 1272) for a reaction time of 30 ms, and the following isolation and fragmentation of [B₁₂I₉(S(CH₃)₂)₂]⁻ ions (m/z 1397) upon CID at a collision energy of 15 arbitrary units. The CID MS³ mass spectrum without further fragmentation of the [B₁₂I₉(S(CH₃)₂)₂]⁻ ions (m/z 1397) is shown on the left and marked with an asterisk. The reagent was dimethyl sulfide. The red arrows highlight the eliminations of CH₃[•], C₂H₄, C₂H₆, and S(CH₃)₂. The elimination of C₂H₆ was not observed in **Figure 3**, where no collision energy was applied to the precursor ion [B₁₂I₉(S(CH₃)₂)₂]⁻.

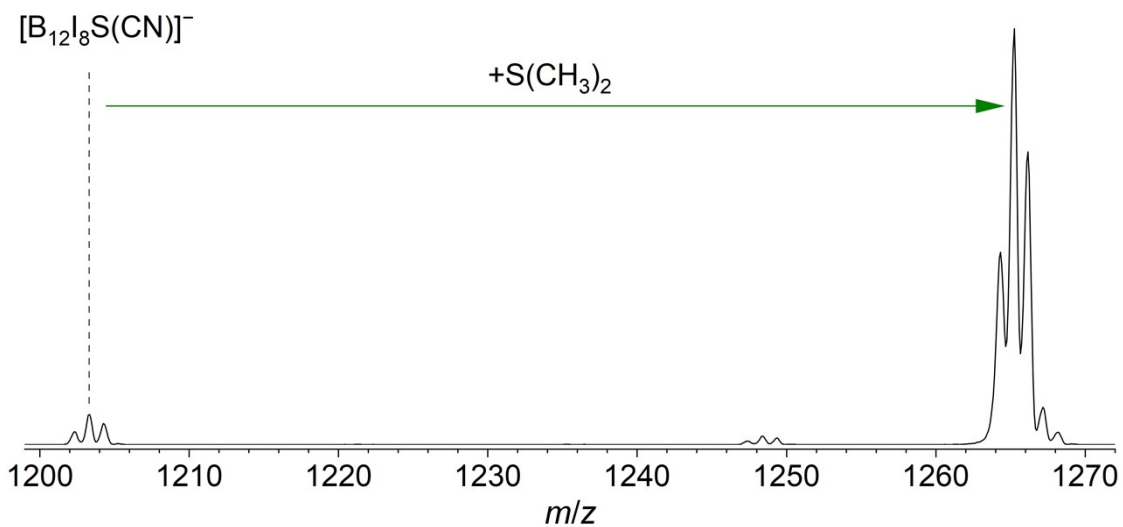


Figure S21. Section of a CID MS² mass spectrum measured after in-source fragmentation of ESI-generated ions from the Cs₂[B₁₂I₁₁(SCN)] solution (CID 35) and the subsequent isolation of [B₁₂I₈S(CN)]⁻ ions (m/z 1203) for a reaction time of 3000 ms with dimethyl sulfide and residual gas. The green arrow highlights the addition reaction with dimethyl sulfide.

5.3 Dimethyl amine

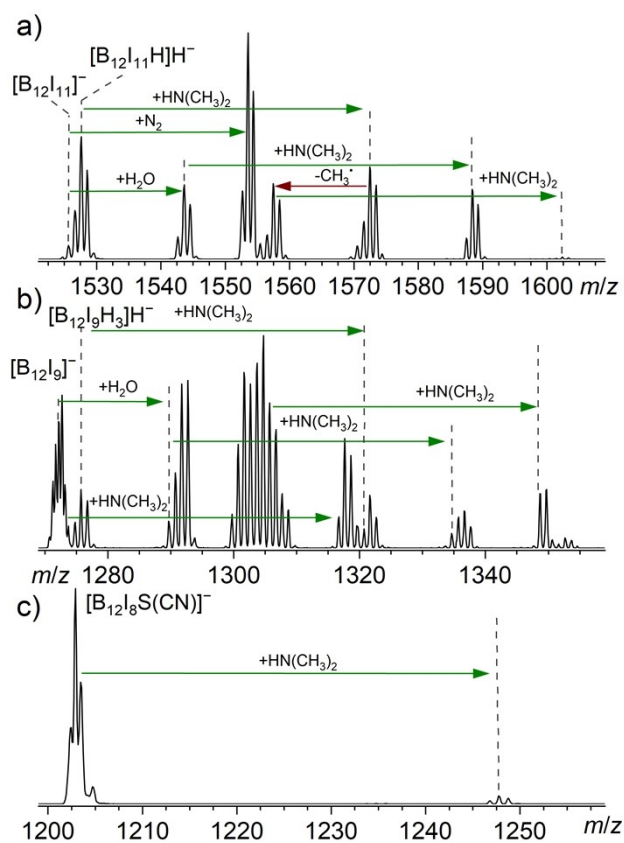


Figure S22. Section of a CID MS² mass spectrum after in-source fragmentation of ESI-generated ions from the $K_2[B_{12}I_{12}]$ solution (CID 40) and subsequent isolation of **a)** $[B_{12}I_{11}]^-$ ions and **b)** $[B_{12}I_9]^-$ ions for a reaction time of 30 ms with dimethyl amine and residual gas. **c)** Section of a CID MS² mass spectrum after in-source fragmentation of ESI-generated ions from the $Cs_2[B_{12}I_{11}(SCN)]$ solution (CID 40) and subsequent isolation of $[B_{12}I_8S(CN)]^-$ ions for a reaction time of 30 ms with dimethyl amine and residual gas. Fragmentation and addition reactions are indicated with red and green arrows, respectively. The elimination of CH_3^\bullet observed in **a)** was verified in a CID MS³ experiment (**Figure S23**). Reaction pathways observed in **b)** are visualized in **Scheme S1**. Note that $[B_{12}I_9]^-$ had completely reacted in **b)** and the doubly charged isotopic pattern of $[B_{24}I_{18}]^{2-}$ ions became visible. $[B_{24}I_{18}]^{2-}$ likely originates from a synthesis side product or a fragment thereof.

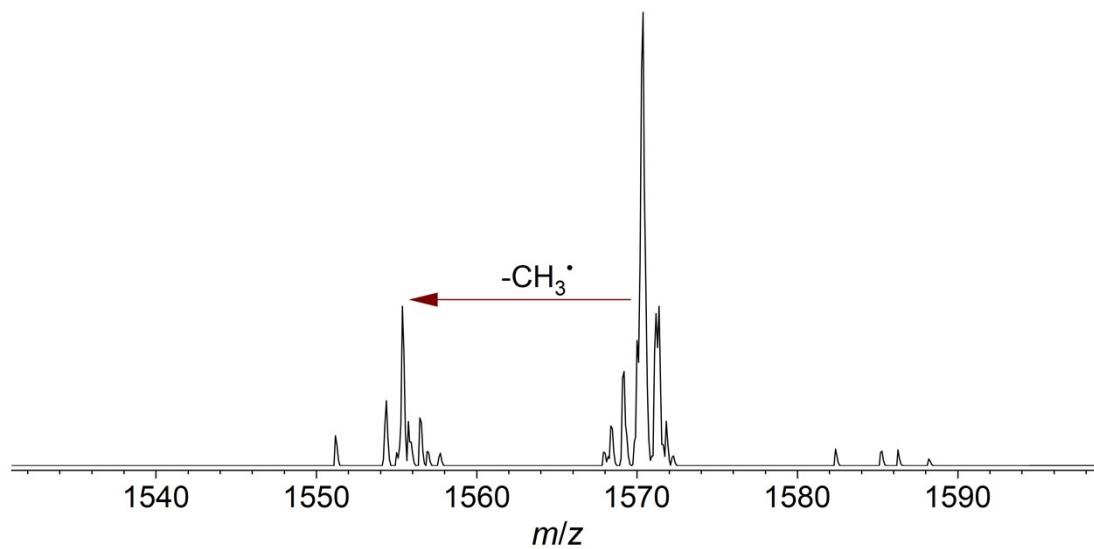
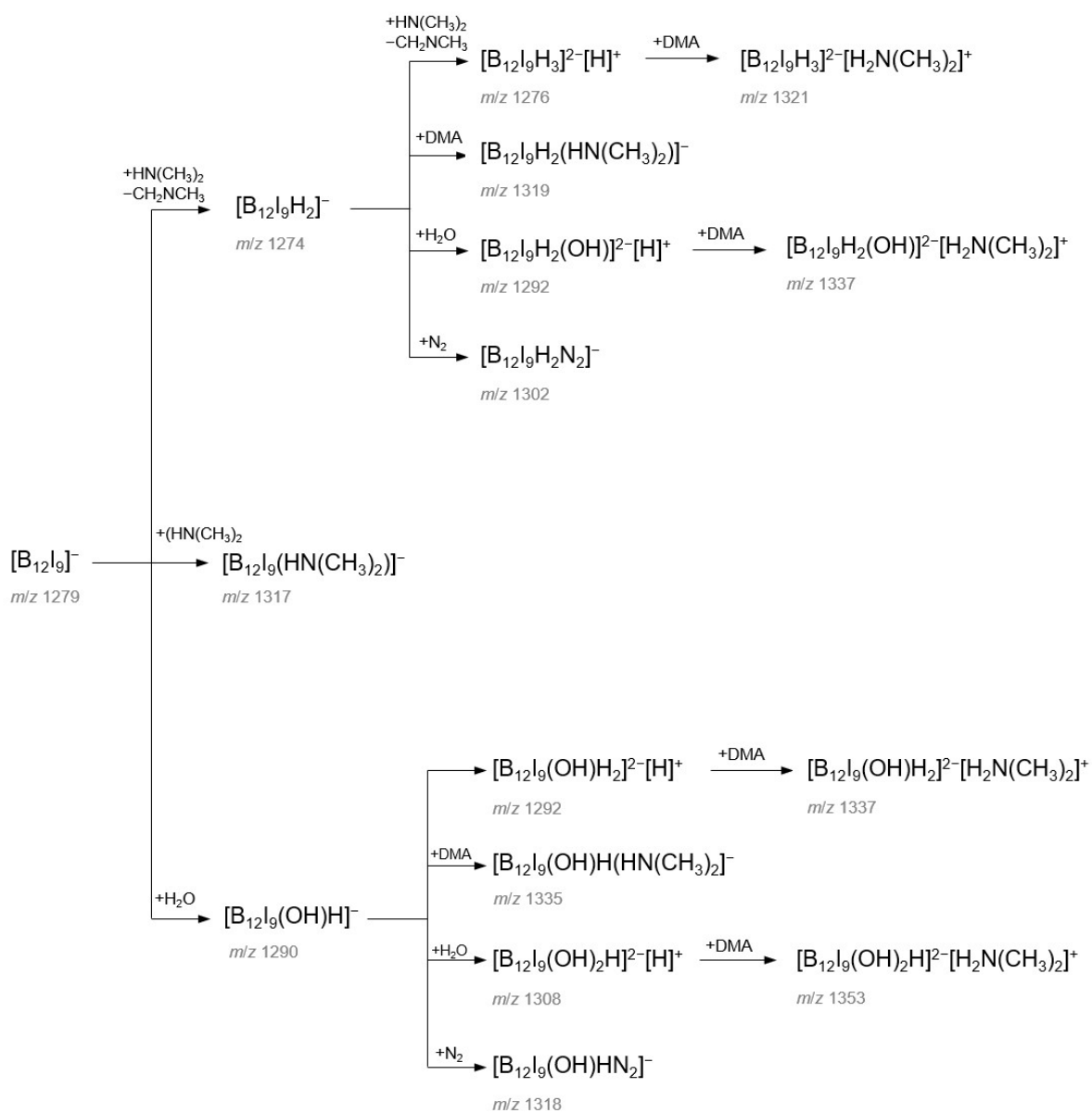


Figure S23. Section of a CID MS³ mass spectrum measured after in-source fragmentation of ESI-generated ions from the K₂[B₁₂I₁₂] solution (CID 40), subsequent isolation of [B₁₂I₁₁]⁻ ions (*m/z* 1526) for a reaction time of 100 ms, and the isolation and fragmentation of [B₁₂I₁₁H]²⁻[H₂N(CH₃)₂]⁺ ions (*m/z* 1571) upon CID at a collision energy of 25 arbitrary units. The reagent was dimethyl amine. The red arrow highlights the elimination of CH₃·.



Scheme S1. Proposed reactions of $[B_{12}I_9]^-$ ions when isolated for a reaction time of 30 ms with dimethyl amine and residual gas.

5.4 Without introduction of neutral reagent

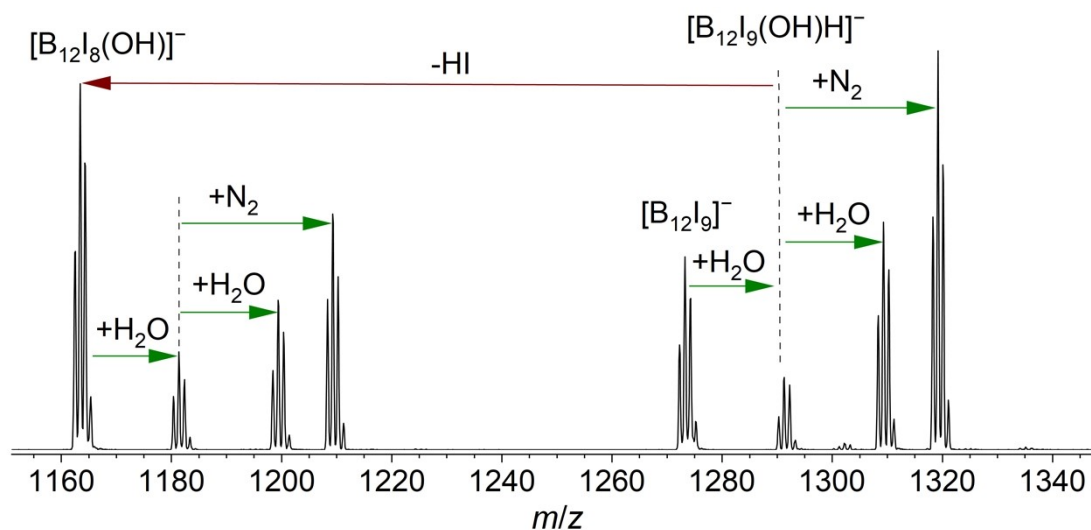


Figure S24. Section of a CID MS² mass spectrum measured after in-source fragmentation of ESI-generated ions from the K₂[B₁₂I₁₂] solution (CID 40) and subsequent isolation [B₁₂I₉]⁻ ions (m/z 1272) for a reaction time of 30 ms with residual gas. Fragmentation and addition reactions are indicated with red and green arrows, respectively.

5.5 Comparison of cyclohexane, dimethyl sulfide, and dimethyl amine

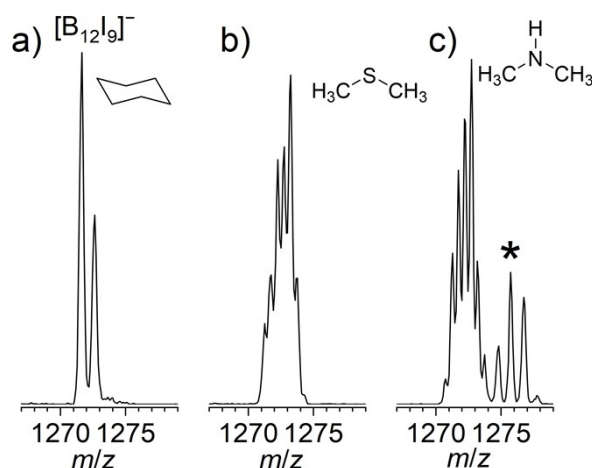


Figure S25. Section of the mass spectrum measured after isolation of [B₁₂I₉]⁻ ions for a reaction time of 30 ms with **a)** cyclohexane, **b)** dimethyl sulfide, and **c)** dimethyl amine. For the amine, the formation of [B₁₂I₉H₃]²⁻[H]⁺ was observed, which was not the case for cyclohexane and dimethyl sulfide. Note that in cases **b)** and **c)**, [B₁₂I₉]⁻ had completely reacted and the double-charged isotopic pattern of [B₂₄I₁₈]²⁻ became visible. The signal assigned to [B₂₄I₁₈]²⁻ ions overlaps with that assigned to [B₁₂I₉]⁻ ions in **a)** and likely originates from a synthesis side product or fragments thereof.

6 LESA mass spectrometry

All mass spectra obtained by LESA were recorded with an LTQ XL Orbitrap mass spectrometer. Note that MS³ experiments for further fragmentation of [B₁₂I₁₁(alkyl chain)]²⁻ are shown in Ref [1] and were not repeated here.

Table S8. Signal assignment for mass spectra shown in **Figure 4**.

| | Experimental <i>m/z</i> value | Assigned molecular formula |
|--|----------------------------------|--|
| [B ₁₂ I ₈ (CN)] ⁻ | 638.6795 | [(B ₁₂ I ₈ (SH)(CN)H) ₂ (C ₄ H ₈ (COO) ₂)] ⁴⁻ |
| | 670.7094 | [(B ₁₂ I ₈ (SH)(CN)H)(B ₁₂ I ₈ (SH)(CN)(OH))(C ₄ H ₈ (COO)(COOC ₈ H ₁₆))] ⁴⁻ |
| | 684.1706 | [B ₁₂ I ₈ (SH)(CN)(C ₆ H ₄ (COO) ₂)] ²⁻ |
| | 731.2564 | [B ₁₂ I ₈ (SH)(CN)H(C ₄ H ₈ (COOC ₈ H ₁₇)(COO))] ²⁻ |
| | 739.2540 | [B ₁₂ I ₈ (SH)(CN)(OH)(C ₄ H ₈ (COOC ₈ H ₁₇)(COO))] ²⁻ |
| | 748.2485 | [B ₁₂ I ₈ (SH)(CN)H(C ₆ H ₄ (COOC ₉ H ₁₉)(COO))] ²⁻ |
| | 756.2458 | [B ₁₂ I ₈ (SH)(CN)(OH)(C ₆ H ₄ (COOC ₉ H ₁₉)(COO))] ²⁻ |
| | 795.3165 | [B ₁₂ I ₈ (SH)(CN)(OH)(C ₄ H ₈ (COOC ₈ H ₁₇)(COOC ₈ H ₁₆))] ²⁻ |
| | 819.3158 | [B ₁₂ I ₈ (SH)(CN)(OH)(C ₆ H ₄ (COOC ₉ H ₁₉)(COOC ₉ H ₁₈))] ²⁻ |
| [B ₁₂ I ₉] ⁻ | 570.6739 | [B ₁₀ I ₈ (OH)H] ²⁻ |
| | 578.6713 | [B ₁₀ I ₈ (OH) ₂] ²⁻ |
| | 584.6799 | [B ₁₁ I ₈ (OH) ₂ H] ²⁻ |
| | 592.6774 | [B ₁₁ I ₈ (OH) ₃] ²⁻ |
| | 599.6852 | [B ₁₁ I ₈ (OH) ₂ (OCH ₃)] ²⁻ |
| | 606.6834 | [B ₁₂ I ₈ (OH) ₄] ²⁻ |
| | 613.6913 | [B ₁₂ I ₈ (OH) ₃ (OCH ₃)] ²⁻ |
| | 637.6419 | [B ₁₂ I ₉ H ₃] ²⁻ |
| | 645.6393 | [B ₁₂ I ₉ (OH)H ₂] ²⁻ |
| | 653.6368 | [B ₁₂ I ₉ (OH) ₂ H] ²⁻ |
| | 708.6552 | [B ₁₂ I ₉ H(C ₄ H ₈ (COO) ₂)] ²⁻ |
| | 781.7099 | [B ₁₂ I ₉ H(C ₆ H ₄)(COO)(COOC ₉ H ₁₈))] ²⁻ |
| | 829.7857 | [B ₁₂ I ₉ (OH)H(C ₄ H ₈ (COOC ₈ H ₁₇)(COOC ₈ H ₁₆))] ²⁻ |
| | 853.7857 | [B ₁₂ I ₉ (OH)H(C ₆ H ₄ (COOC ₉ H ₁₉)(COOC ₉ H ₁₈))] ²⁻ |
| [B ₁₂ I ₁₁] ⁻ | 763.5337 | [B ₁₂ I ₁₁ H] ²⁻ |
| | 771.5312 | [B ₁₂ I ₁₁ (OH)] ²⁻ |
| | 947.6796 | [B ₁₂ I ₁₁ (C ₄ H ₈ (COOC ₈ H ₁₇)(COOC ₈ H ₁₆))] ²⁻ |
| | 971.6798 | [B ₁₂ I ₁₁ (C ₆ H ₄ (COOC ₉ H ₁₉)(COOC ₉ H ₁₈))] ²⁻ |

6.1 Background

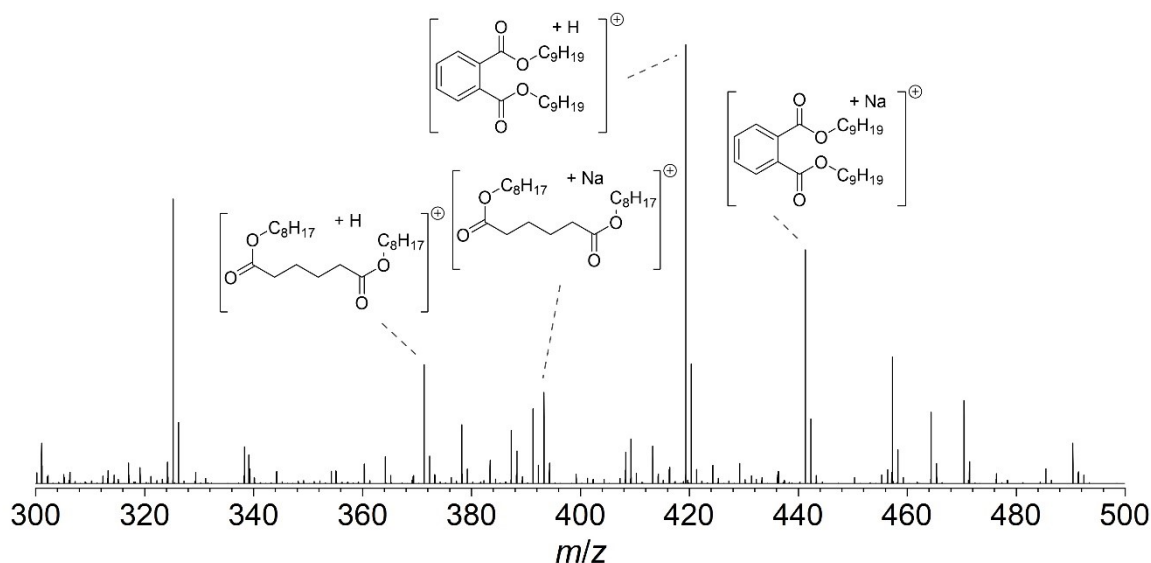


Figure S26. Mass spectrum in positive ion mode obtained with LESA after the deposition of $[\text{B}_{12}\text{I}_{12}]^{2-}$ ions on p-doped Si (44 pmol). Molecular structures are assigned to nonyl phthalate and dioctyl adipate.

6.2 $[\text{B}_{12}\text{I}_{11}]^-$

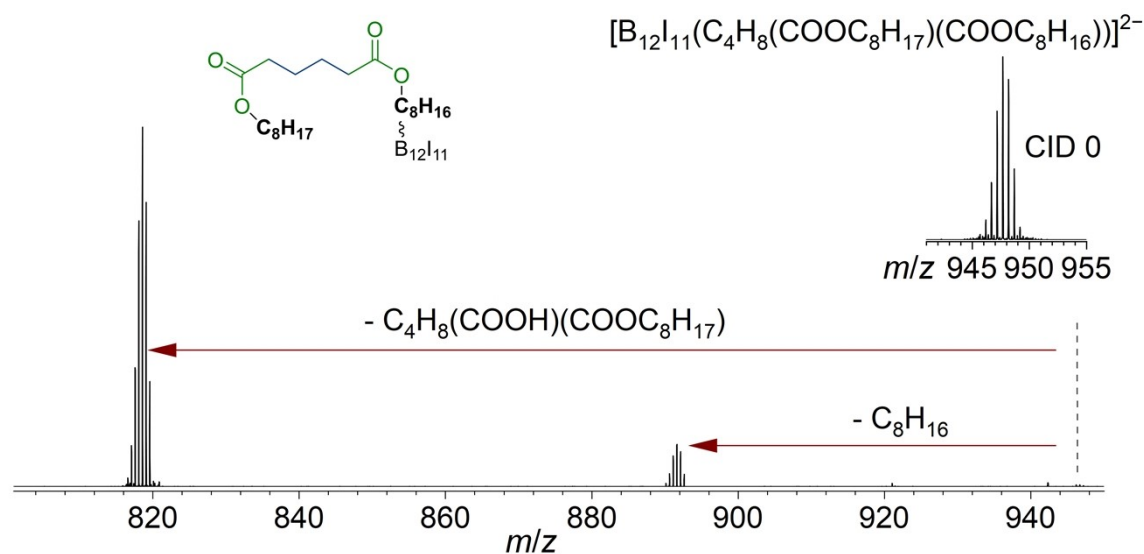


Figure S27. Section of a CID MS^2 mass spectrum obtained with LESA after the deposition of $[\text{B}_{12}\text{I}_{11}]^-$ ions on p-doped Si (52 pmol). $[\text{B}_{12}\text{I}_{11}(\text{C}_4\text{H}_8(\text{COOC}_8\text{H}_{17})(\text{COOC}_8\text{H}_{16}))]^{2-}$ ions (m/z 947.7) were isolated and fragmented upon CID at a collision energy of 15 arbitrary units. The assigned molecular structure is adopted from **Figure 4a**. Eliminations are indicated with a red arrow. A section of a mass spectrum obtained after isolation of $[\text{B}_{12}\text{I}_{11}(\text{C}_4\text{H}_8(\text{COOC}_8\text{H}_{17})(\text{COOC}_8\text{H}_{16}))]^{2-}$ ions (m/z 947.7) is shown in the top right corner.

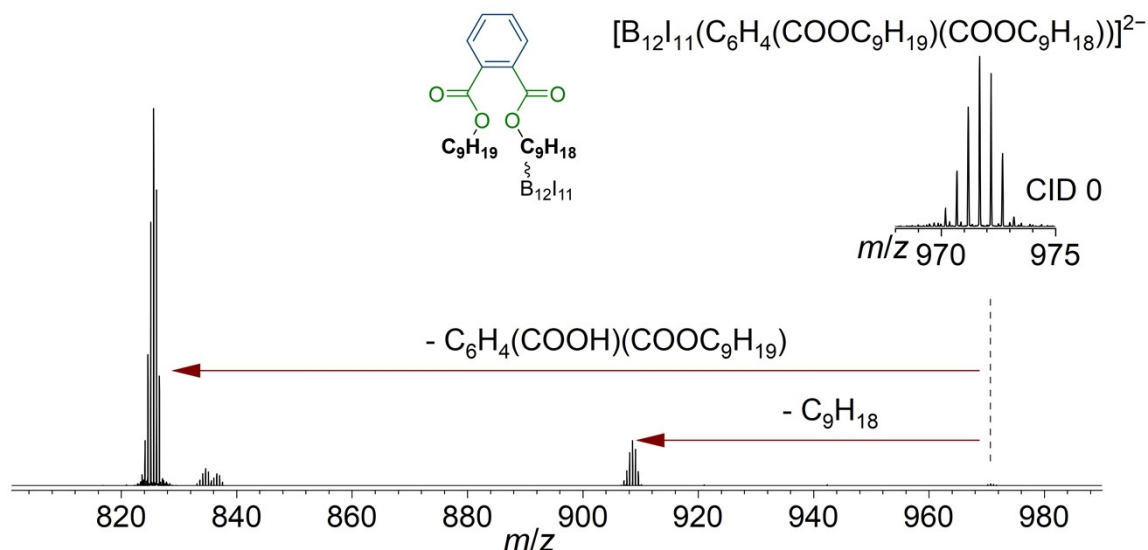


Figure S28. Section of a CID MS² mass spectrum obtained with LESA after the deposition of [B₁₂I₁₁]⁻ ions on p-doped Si (52 pmol). [B₁₂I₁₁(C₆H₄(COOC₉H₁₉)(COOC₉H₁₈))]²⁻ ions (*m/z* 971.7) were isolated and fragmented upon CID at a collision energy of 15 arbitrary units. The assigned molecular structure is adopted from **Figure 4a**. Eliminations are indicated with a red arrow. A section of a mass spectrum obtained after isolation of [B₁₂I₁₁(C₆H₄(COOC₉H₁₉)(COOC₉H₁₈))]²⁻ ions (*m/z* 971.7) is shown in the top right corner.

6.3 [B₁₂I₉]⁻

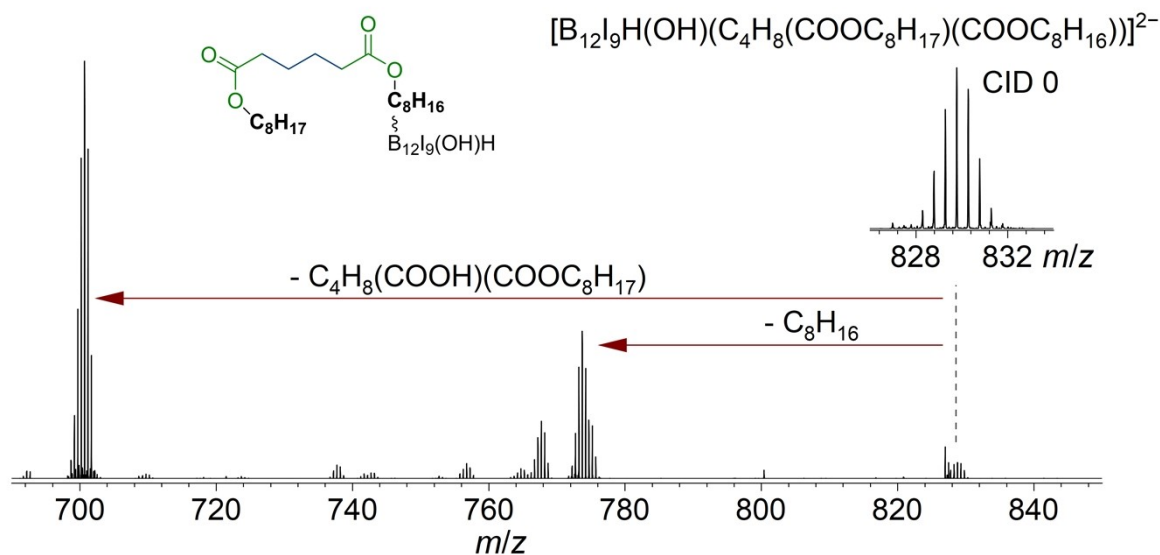


Figure S29. Section of a CID MS² mass spectrum obtained with LESA after the deposition of [B₁₂I₉]⁻ ions on p-doped Si (52 pmol). [B₁₂I₉(OH)H(C₄H₈(COOC₈H₁₇)(COOC₈H₁₆))]²⁻ ions (*m/z* 829.8) were isolated and fragmented upon CID at a collision energy of 10 arbitrary units. The assigned molecular structure is adopted from **Figure 4b**. Eliminations are indicated with a red arrow. A section of a mass spectrum obtained after isolation of [B₁₂I₉(OH)H(C₄H₈(COOC₈H₁₇)(COOC₈H₁₆))]²⁻ ions (*m/z* 829.8) is shown in the top right corner.

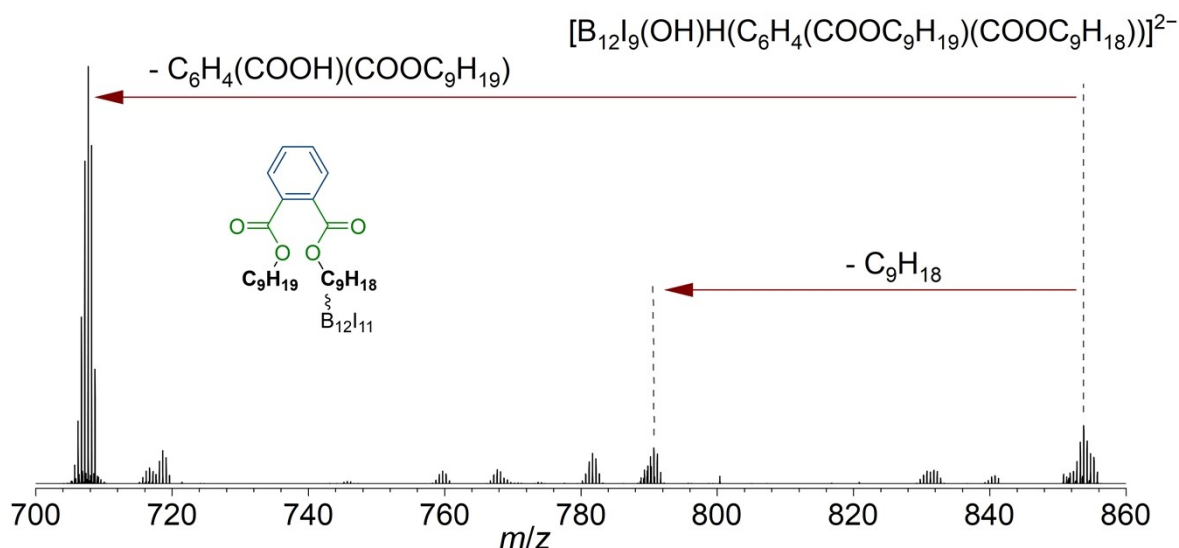


Figure S30. Section of a CID MS² mass spectrum obtained with LESA after the deposition of [B₁₂I₉]⁻ ions on p-doped Si (52 pmol). [B₁₂I₉H(OH)(C₆H₄(COOC₉H₁₉)(COOC₉H₁₈))]²⁻ ions (*m/z* 853.7) were isolated and fragmented upon CID at a collision energy of 15 arbitrary units. The assigned molecular structure is adopted from **Figure 4b**. Eliminations are indicated with a red arrow.

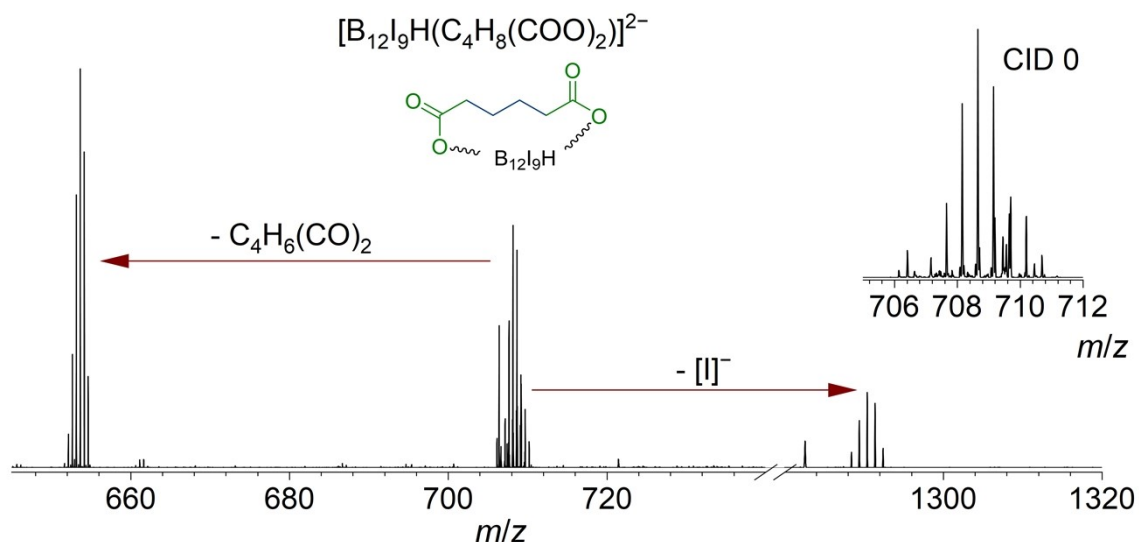


Figure S31. Section of a CID MS² mass spectrum obtained with LESA after the deposition of [B₁₂I₉]⁻ ions on p-doped Si (52 pmol). [B₁₂I₉H(C₄H₈COOCOO)]²⁻ ions (*m/z* 708.7) were isolated and fragmented upon CID at a collision energy of 15 arbitrary units. The assigned molecular structure is adopted from **Figure 4b**. Eliminations are indicated with a red arrow. A section of a mass spectrum obtained after isolation of [B₁₂I₉H(C₄H₈COOCOO)]²⁻ ions (*m/z* 708.7) is shown in the top right corner.

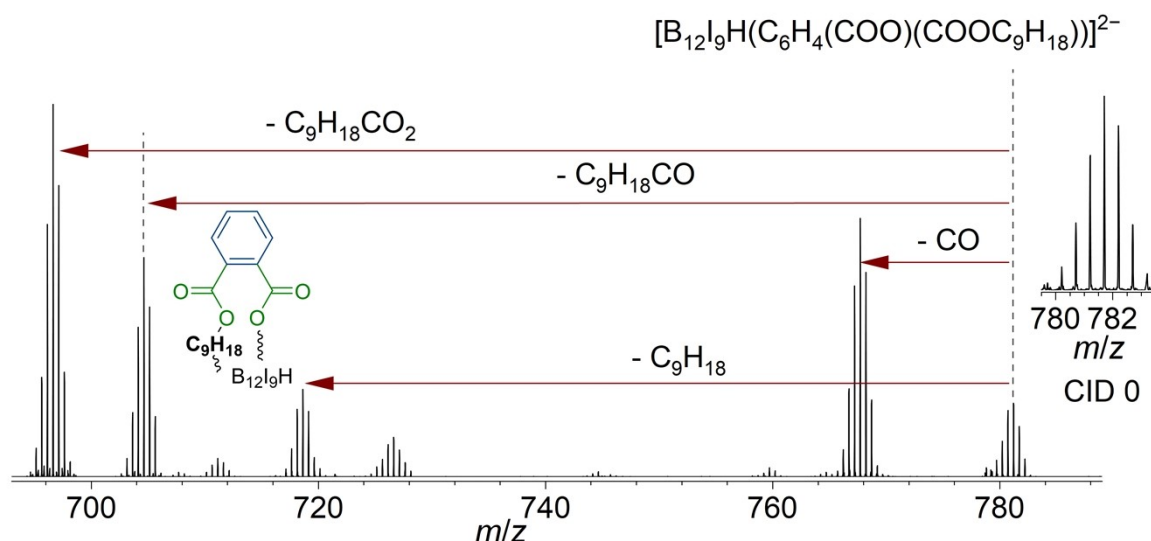


Figure S32. Section of a CID MS² mass spectrum obtained with LESA after the deposition of $[B_{12}I_9]^-$ ions on p-doped Si (52 pmol). $[B_{12}I_9H(C_6H_4)(COO)(COOC_9H_{18})]^{2-}$ ions (m/z 781.7) were isolated and fragmented upon CID at a collision energy of 15 arbitrary units. The assigned molecular structure is adopted from **Figure 4b**. Eliminations are indicated with a red arrow. A section of a mass spectrum obtained after isolation of $[B_{12}I_9H(C_6H_4)(COO)(COOC_9H_{18})]^{2-}$ ions (m/z 781.7) is shown on the right.

6.4 $[B_{12}I_8S(CN)]^-$

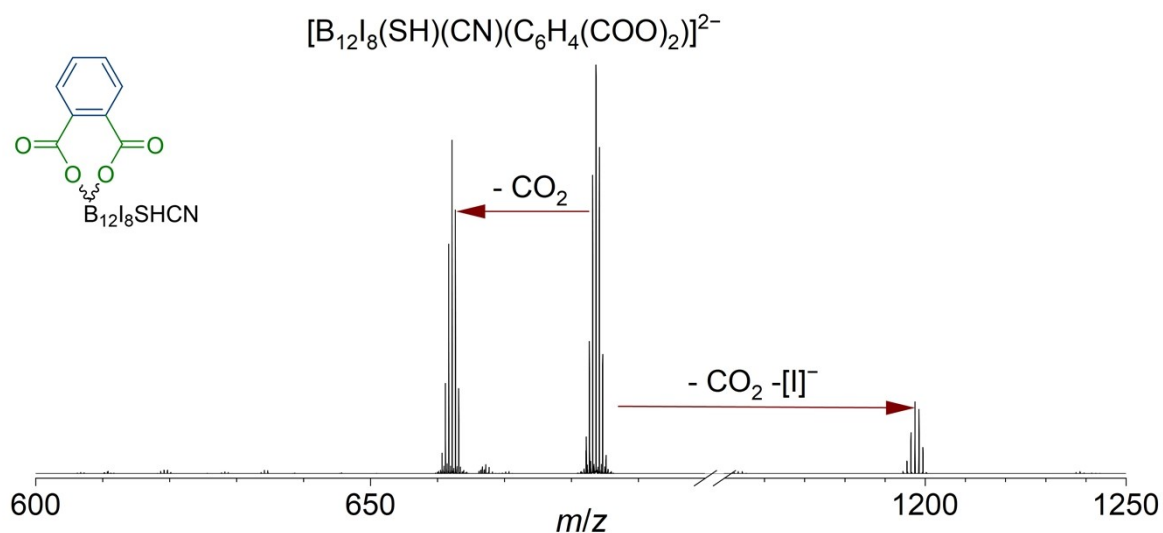


Figure S33. Section of a CID MS² mass spectrum obtained with LESA after the deposition of $[B_{12}I_8S(CN)]^-$ ions on p-doped Si (207 pmol). $[B_{12}I_8(SH)(CN)(C_6H_4(COO)_2)]^{2-}$ ions (m/z 684.2) were isolated and fragmented upon CID at a collision energy of 20 arbitrary units. The assigned molecular structure is adopted from **Figure 4c**. Eliminations are indicated with a red arrow.

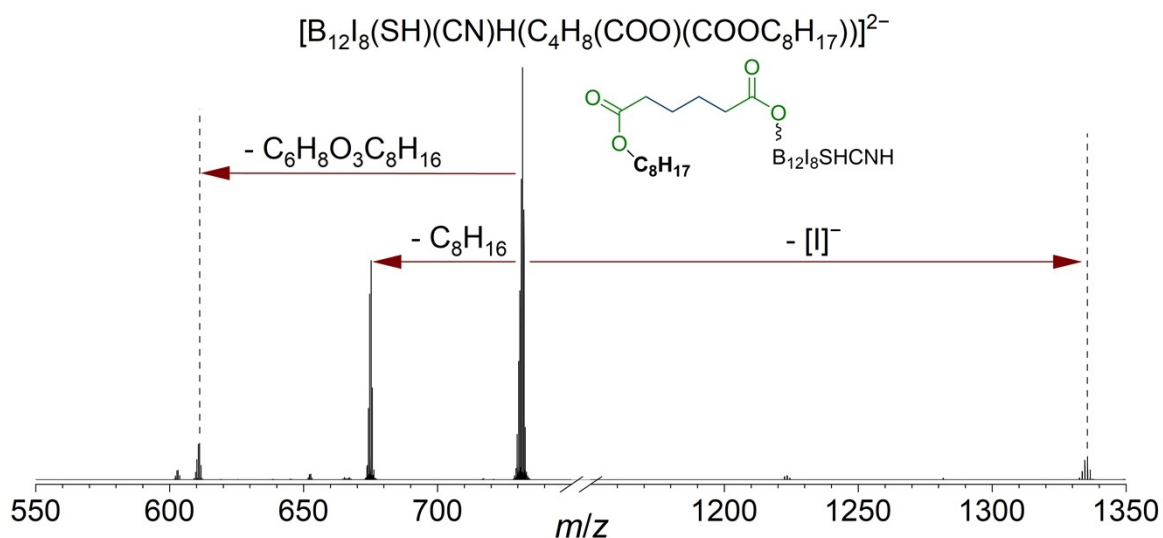


Figure S34. Section of a CID MS² mass spectrum obtained with LESA after the deposition of $[B_{12}I_8S(CN)]^-$ ions on p-doped Si (207 pmol). $[B_{12}I_8(CN)(SH)H(C_4H_8(COO)(COOC_8H_{17}))]^{2-}$ ions (m/z 731.3) were isolated and fragmented upon CID at a collision energy of 10 arbitrary units. The assigned molecular structure is adopted from **Figure 4c**. Eliminations are indicated with a red arrow.

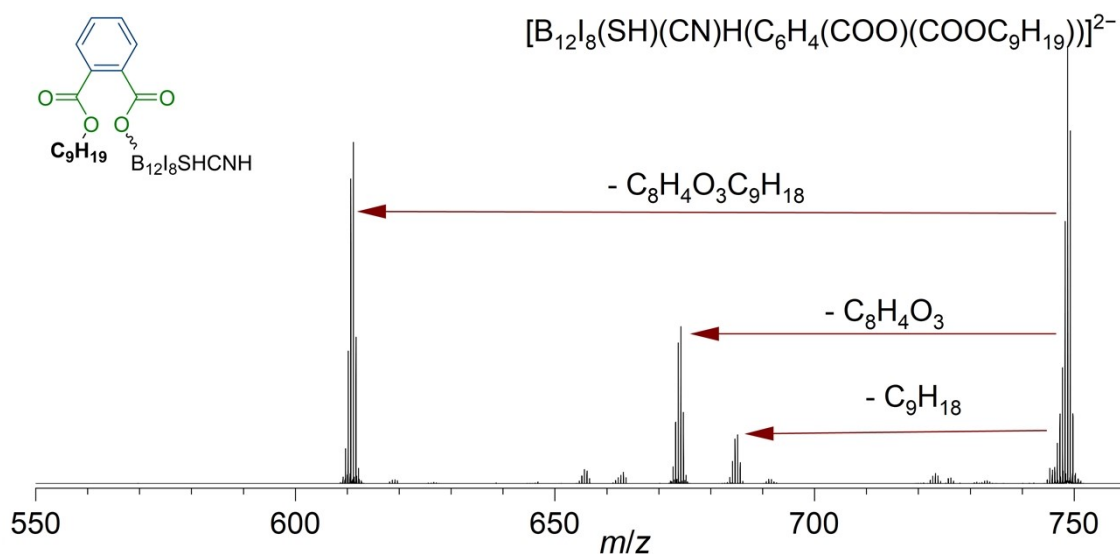


Figure S35. Section of a CID MS² mass spectrum obtained with LESA after the deposition of $[B_{12}I_8S(CN)]^-$ ions on p-doped Si (207 pmol). $[B_{12}I_8(CN)(SH)H(C_6H_4(COO)(COOC_9H_{19}))]^{2-}$ ions (m/z 748.2) were isolated and fragmented upon CID at a collision energy of 10 arbitrary units. The assigned molecular structure is adopted from **Figure 4c**. Eliminations are indicated with a red arrow.

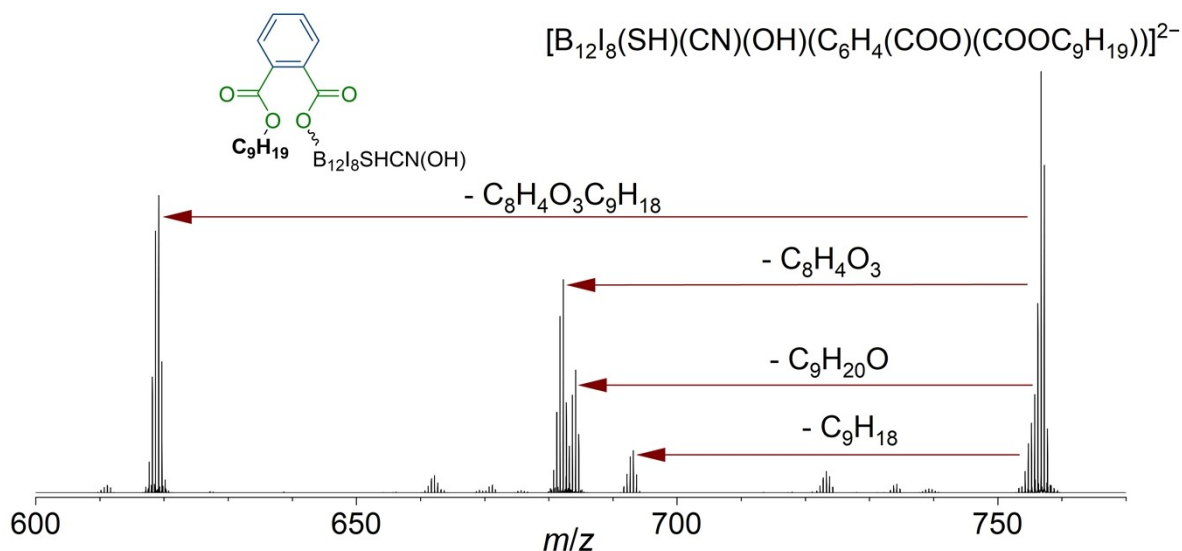


Figure S36. Section of a CID MS² mass spectrum obtained with LESA after the deposition of $[B_{12}I_8S(CN)]^-$ ions on p-doped Si (207 pmol). $[B_{12}I_8(CN)(SH)(OH)(C_6H_4(COO)(COOC_9H_{19}))]^{2-}$ ions (m/z 756.2) were isolated and fragmented upon CID at a collision energy of 10 arbitrary units. The assigned molecular structure is adopted from **Figure 4c**. Eliminations are indicated with a red arrow.

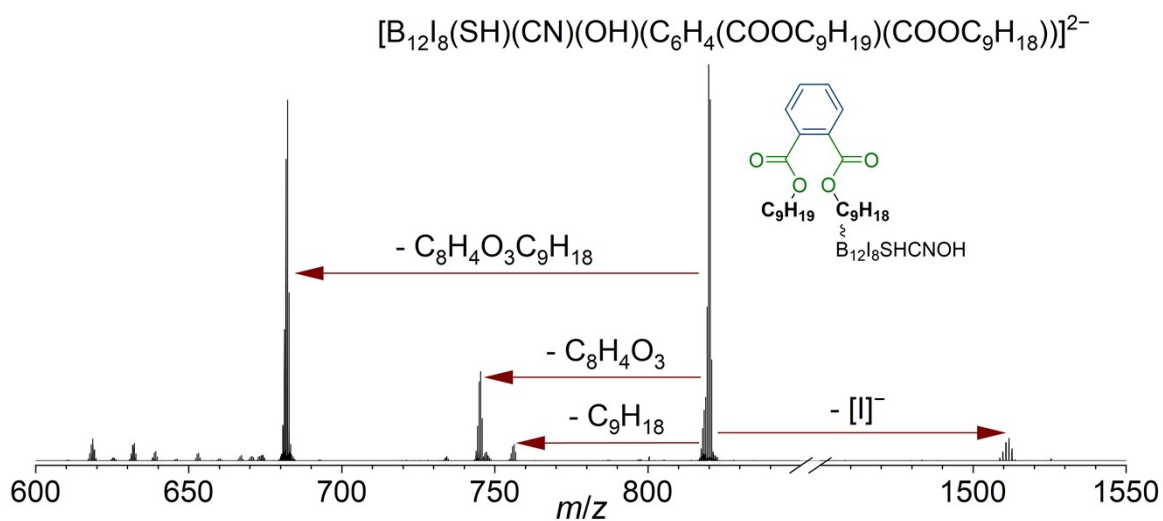


Figure S37. Section of a CID MS² mass spectrum obtained with LESA after the deposition of $[B_{12}I_8S(CN)]^-$ ions on p-doped Si (207 pmol). $[B_{12}I_8(CN)(SH)(OH)(C_6H_4(COOC_9H_{19})(COOC_9H_{18}))]^{2-}$ ions (m/z 819.3) were isolated and fragmented upon CID at a collision energy of 10 arbitrary units. The assigned molecular structure is adopted from **Figure 4c**. Eliminations are indicated with a red arrow.

7 Ion soft-landing settings

Table S9. Optimized voltage and pressure settings.

| Voltages / V | [B ₁₂ I ₈ S(CN)] ⁻ | [B ₁₂ I ₉] ⁻ | [B ₁₂ I ₁₁] ⁻ |
|---------------------|---|--|---|
| ESI | -3500.00 | -3100.00 | -3200.00 |
| Inlet 1 | -400.00 | -380.00 | -380.00 |
| Inlet 2 | -400.00 | -400.00 | -400.00 |
| Ionfunnel 1a | -400.00 | -400.00 | -400.00 |
| Ionfunnel 1b | -310.00 | -270.00 | -270.00 |
| Ionfunnel 1c | -290.00 | -300.00 | -300.00 |
| Ionfunnel 1d | -177.00 | -200.00 | -200.00 |
| Ionfunnel2a | -184.80 | -221.00 | -221.00 |
| Ionfunnel 2 lens | -119.00 | -127.00 | -127.00 |
| Ionfunnel 2b | -119.00 | -117.00 | -95.00 |
| Collision cell bias | -6.10 | -6.50 | -6.50 |
| Collision cell lens | -6.00 | -6.20 | -6.20 |
| Ion guide bias | -5.80 | -1.90 | -1.90 |
| Ion guide lens | 10.50 | 80.00 | 80.00 |
| Mass filter in | 36.40 | 60.00 | 60.00 |
| Mass filter pre | 30.00 | 40.00 | 40.00 |
| mass filter bias | 19.90 | 20.00 | 16.00 |
| Mass filter post | 19.00 | 43.00 | 43.00 |
| Mass filter out | 1.00 | -6.00 | -6.00 |
| Drive / % | | | |
| Ion funnel 1 | 35.00 | 43.00 | 43.00 |
| Ion funnel 2 | 30.00 | 30.00 | 30.00 |
| Collision cell | 44.00 | 42.00 | 42.00 |
| Ion guide | 28.00 | 17.00 | 17.00 |
| Pressure / mbar | | | |
| Ion funnel 1 | 9.7 | 9.8 | 9.8 |
| Ion funnel 2 | 3.1 | 3.2 | 3.2 |

8 Measurement of kinetic energy

The kinetic energy distribution of deposited ions was determined using the retarding potential method.^[2] A double copper mesh combined with a detection metal plate was positioned behind the quadrupole. The first mesh was grounded, whereas a variable DC voltage (retarding potential) was applied to the second mesh. The ion current was recorded as a function of the retarding potential (step size 0.1 V, data point recorded every 150 ms). The graph was fitted with a sigmoidal Boltzmann distribution. The inflection point is assigned to the maximum of the kinetic energy distribution per charge (KE / charge number). An example graph is shown in **Figure S37**. The measurement was repeated four times for each ion with the ion soft-landing settings shown in **Table S9**. The averaged values are shown in **Table S10**.

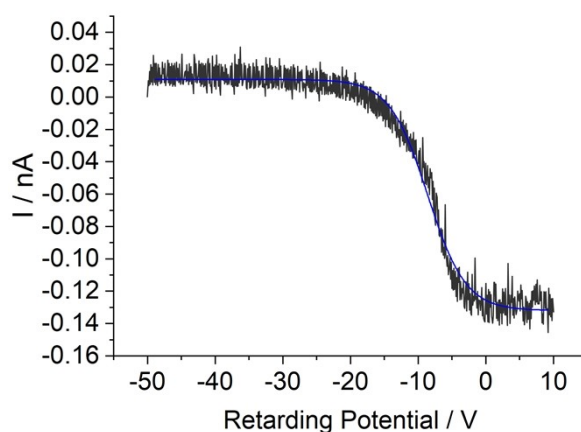


Figure S37. Recorded ion current as a function of the retarding potential.

Table S10. Maximum of the kinetic energy distribution of deposited ions in eV / z.

| Deposited ions | Maximum of kinetic energy distribution |
|--|--|
| $[\text{B}_{12}\text{I}_8\text{S}(\text{CN})]^-$ | 8.7 |
| $[\text{B}_{12}\text{I}_9]^-$ | 10.1 |
| $[\text{B}_{12}\text{I}_{11}]^-$ | 8.2 |

9 References

- [1] J. Warneke, M. Mayer, M. Rohdenburg, X. Ma, J. K. Y. Liu, M. Grellmann, S. Debnath, V. A. Azov, E. Apra, R. P. Young et al., *Proc. Natl. Acad. Sci. U.S.A.* **2020**, *117*, 23374.
- [2] H. Y. Samayoa-Oviedo, K.-A. Behrend, S. Kawa, H. Knorke, P. Su, M. E. Belov, G. Anderson, J. Warneke, J. Laskin, *Anal. Chem.* **2021**, *93*, 14489.